An integrated pan-tropical biomass map using multiple reference datasets

Avitabile V. [1], Herold M. [1], Heuvelink G.B.M. [1], Lewis S.L. [2,3], Phillips O.L. [2], Asner G. P. [4], Asthon P., Banin L.F.[5], Bayol N. [6], Berry N.[12], Boeckx P., de Jong B. [7], DeVries B. [1], Girardin C. [8], Kearsley E. [9], Lindsell J [10], Lopez-Gonzalez G. [2], Lucas R. [11], Malhi Y. [8], Morel A. [8], Mitchard E. [12], Nagy L., Qie L.[2], Quinones M. [13], Ryan C. [12], Slik F., Sunderland, T., Vaglio Laurin G. [14], Valentini R. [15], Verbeeck H. [9], Wijaya A. [16], Willcock S. [17]

(1). Wageningen University, the Netherlands; (2). University of Leeds, UK; (3).Universtity College London, UK; (4). Carnegie Institution for Science, USA; (5). Centre for Ecology and Hydrology, UK. (6). Foret Ressources Management, France; (7). Ecosur, Mexico; (8). University of Oxford, UK; (9) Ghent University, Belgium; (10). The RSPB Centre for Conservation Science, UK.; (11). Aberystwyth University, Australia; (12). University of Edinburgh, UK; (13). SarVision, the Netherlands; (14). Centro Euro-Mediterraneo sui Cambiamenti Climatici, Italy; (15). Tuscia University, Italy; (16). Center for International Forestry Research, Indonesia; (17). University of Southampton, UK;

Abstract

We combined two existing biomass datasets (input maps) into a pan-tropical biomass map at 1 km resolution using an unprecedented reference dataset and a data fusion approach, achieving lower errors than the input maps and almost unbiased estimates at the continental scale. A variety of field observations and locally-calibrated high-resolution biomass maps - not used by the input maps - were harmonized and upscaled to the map resolution, providing 15,969 biomass estimates at 1 km resolution (reference dataset). The input maps were integrated using a data fusion approach based on bias removal and weighted linear averaging that incorporates and spatializes the biomass patterns indicated by the reference data. The method was applied independently in areas (strata) with homogeneous error patterns of the input maps, which were estimated from the reference data and additional covariates. The fused map showed biomass stocks for the tropics 15% and 19% lower than the two input maps, and a different spatial pattern. Compared to the input maps, the fused map shows higher biomass density in the dense forest areas in the Congo basin, West Africa Eastern Amazon and South-East Asia, and lower values in Central America and in most dry vegetation areas of Africa. The validation exercise, based on 3,619 estimates from the reference

dataset not used in the fusion process, showed that the fused map had a RMSE 8 – 74% lower than that of the input maps and, most importantly, nearly unbiased estimates (mean bias 4 Mg dry mass ha^{-1} vs. 21 and 28 Mg ha^{-1} for the input maps). The fusion method can be applied at any scale including the policy-relevant national level, where it can provide improved biomass estimates by integrating existing regional biomass maps as input maps and additional, country-specific reference datasets.

Keywords: aboveground biomass, carbon cycle, forest plots, tropical forest, forest inventory, REDD+, satellite mapping, remote sensing,

Introduction

Recently, considerable efforts have been made to better quantify the amounts and spatial distribution of aboveground biomass, a key parameter for estimating carbon emissions and removals due to land-use change, and related impacts on climate (Baccini et al., 2012; Harris et al., 2012; Houghton et al., 2012; Saatchi et al. 2011; Mitchard et al. 2014). Particular attention has been given to the tropical regions, where uncertainties are higher (Ziegler et al., 2012; Grace et al., 2014). In addition to ground observations acquired by research networks or for forest inventory purposes, several biomass maps have been recently produced at different scales, using a variety of empirical modelling approaches based on remote sensing data calibrated by field observations (e.g., Goetz et al., 2011; Birdsey et al., 2013). Biomass maps at moderate resolution have been produced for the entire tropical belt by integrating various satellite observations (Saatchi et al., 2011; Baccini et al., 2012), while higher resolution datasets have been produced at local or national level using medium-high resolution satellite data (e.g., Avitabile et al., 2012; Cartus et al., 2014), sometimes in combination with airborne Light Detection and Ranging (LiDAR) data (Asner et al., 2012a, 2012b, 2013, 2014a). The various datasets often have different purposes: research plots provide a detailed and accurate estimation of biomass (and other ecological parameters or processes) at the local level, forest inventory networks using a sampling approach to obtain statistics of biomass stocks (or growing stock volume) per forest type at the sub-national or national level, while high-resolution biomass maps can provide detailed and spatially explicit estimates of biomass density to assist natural resource management, and large scale datasets depict biomass distribution for global-scale carbon accounting and modelling.

In the context of the United Nations mechanism for Reducing Emissions from Deforestation and forest Degradation (REDD+), emission estimates obtained from spatially explicit biomass datasets may be favoured compared to those based on mean values derived from plot networks. This preference stems from the fact that plot networks are not designed to represent land cover change events, which usually do not occur randomly and may affect forests with biomass density systematically different from the mean value (Baccini and Asner, 2013). With very few tropical countries having national biomass maps or reliable statistics on forest carbon stocks, regional maps may provide advantages compared to the use of default mean values (e.g., IPCC (2006) Tier 1 values) to assess emissions from deforestation, if their accuracy is reasonable and their estimates are not affected by systematic errors (Avitabile et al., 2011). However, these conditions are difficult to assess since proper validation of regional biomass maps remains problematic, given their large area coverage and large mapping unit (Mitchard et al., 2013), while ground observations are only available for a limited number of small sample areas.

The comparison of two recent pan-tropical biomass maps (Saatchi et al., 2011; Baccini et al., 2012) reveals substantial differences between the two products (Mitchard et al., 2013). Further comparison with ground observations and high-resolution maps in the Amazon basin indicated substantially different biomass patterns at regional scales (Mitchard et al., 2014; Baccini and Asner, 2013, Hills et al., 2013). Such comparisons have stimulated a debate over the use and capabilities of different types of biomass products (Saatchi et al., 2014; Langner et al., 2014) and have highlighted both the importance and sometimes the lack of integration of different datasets. On one hand, the two pan-tropical maps are consistent in terms of methodology because both use the same primary data source (GLAS LiDAR) alongside a similar modelling approach to upscale the LiDAR data to larger scales. Moreover, they have the advantage of being calibrated using hundreds of thousands of biomass estimates derived from height metrics computed by a spaceborne LiDAR sensor distributed over the tropics. However, such maps are based on remotely sensed variables that do not directly measure biomass, but are sensitive to canopy cover and canopy height parameters that do not fully capture the biomass variability of complex tropical forests. Furthermore, both products assume global or continental allometric relationships in which biomass varies only with stand height, and further errors are introduced by upscaling the calibration data to the coarser satellite data. On the other hand, ground plots use allometric equations to estimate biomass at individual tree level using directly measurable parameters such as diameter, height and species identity (hence wood density). However, they have limited coverage, are not error-free, and compiling various datasets over large areas is made more complex due to differing sampling strategies (e.g., stratification (or not) of

landscapes, plot size, minimum diameter of trees measured). Considering the rapid increase of biomass observations at different scales and the different capabilities and limitations of the various datasets, it is becoming more and more important to identify strategies that are capable of making best use of existing information and optimally integrate various data sources for improved large area biomass assessment (e.g., see Willcock et al. 2012).

In the present study, we compiled existing ground observations and high-resolution biomass maps to obtain a reference dataset of high quality aboveground biomass data for the tropical region, including both plot data and high-resoltion biomass maps (objective 1). This reference dataset was used to assess the two pan-tropical biomass maps (objective 2) and to combine them in a fused map that optimally integrates the two maps, based on the method presented by Ge et al. (2014) (objective 3). Lastly, the fused map was compared to known biomass patterns and stocks across the tropics (objective 4).

Overall, the approach consisted of pre-processing, screening and harmonizing the Saatchi and Baccini maps (called 'input maps'), the high-resolution biomass maps (called 'reference maps') and the field plots (called 'reference plots'; 'reference dataset' refers to the maps and plots combined) to a common spatial resolution and geospatial reference system (Figure 1). The input maps were combined using bias removal and weighted linear averaging ('fusion'). The fusion model was applied independently in areas representing different error patterns of the input maps (called 'error strata'), which were estimated from the reference data and additional covariates (called 'covariate maps'). The reference dataset included only a subset of the reference maps (i.e., the cells with highest confidence) and if a stratum was lacking reference data ('reference data gaps'), additional data were extracted from the reference maps ('consolidation'). The fused map was validated using independent data and its uncertainty quantified using model parameters. In this study, the term biomass refers to aboveground live woody biomass and is reported in units of Mg dry mass ha^{-1}.

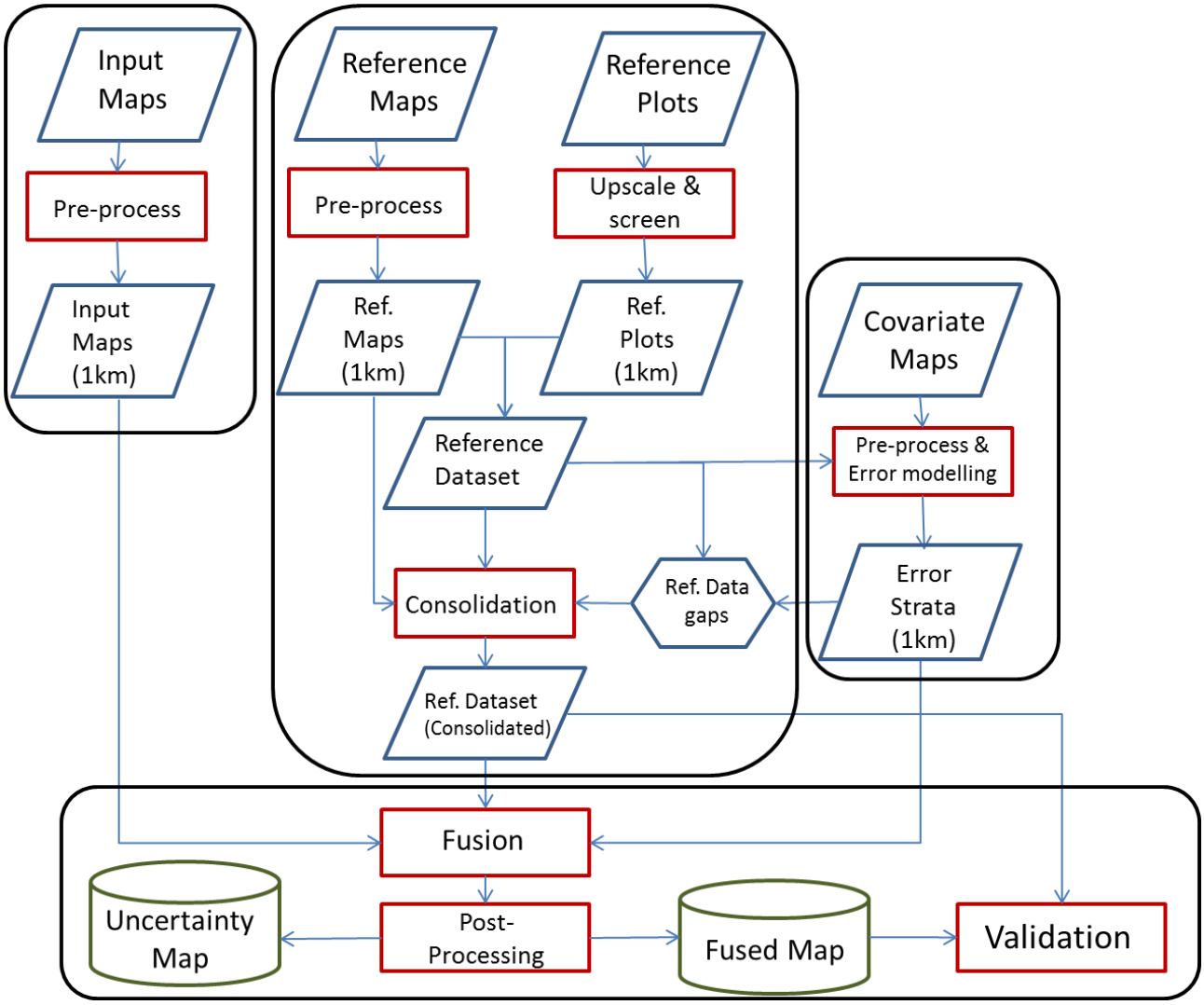

Figure 1: methodology flowchart

Data & Methods

Input maps

The input maps used for this study were the two pan-tropical datasets published by Saatchi et al. (2011) and Baccini et al. (2012), hereafter referred to as the Saatchi and Baccini maps individually, or collectively as input maps. The Baccini map was provided in MODIS sinusoidal projection with a spatial resolution of 463 m while the Saatchi map is in a geographic projection (WGS-84) at 0.00833 degrees (c. 1 km) pixel size. The two datasets were harmonized by first projecting the Baccini map to the coordinate system of the Saatchi map using the Geospatial Data Abstraction Library (www.gdal.org) and then aggregating to match its spatial resolution and grid. Spatial aggregation was performed by computing the mean value of the pixels whose centre was located

within each 1 km cell of the Saatchi map. Resampling was then undertaken using the nearest neighbor method.

Reference dataset

The reference dataset comprised individual tree-based field data and high-resolution biomass maps. The field data included biomass estimates derived from field measurement of tree parameters and allometric equations. The biomass maps included high-resolution (≤ 100 m) datasets derived from satellite data using empirical models calibrated and validated using local ground observations and, in some cases, airborne LiDAR measurements (Table S7 – S10). Given the variability of procedures used to acquire and produce the various datasets, they were first screened according to a set of quality criteria to select only the most reliable biomass estimates, and then pre-processed to be harmonized with the pan-tropical biomass maps in terms of spatial resolution and variable observed. Field and map datasets providing aboveground carbon density were converted to biomass units using the same coefficients used for their original conversion from biomass to carbon. The sources of the reference data are listed in table S7 and S9.

Data screening and pre-processing

Reference field data

The reference field data included ground observations in forest inventory plots, for which accurate geolocation and biomass estimates were available. The pre-processing of the data consisted of a 2-step screening and a harmonization procedure. A preliminary screening selected only the ground data that estimated aboveground biomass of all living trees with diameter at breast height ≥ 5-10 cm, and acquired on or after the year 2000. The taxonomic identities of trees strongly indicate wood density and hence stand-level biomass (e.g., Baker et al., 2004; Mitchard et al. 2014). Plots were therefore only selected if tree biomass was estimated using at least tree diameter and wood density as input parameters, and plot coordinates were measured using a GPS. All datasets not conforming to these requirements or not providing clear information on the biomass pool measured, the tree parameters measured in the field, the allometric model applied, the year of measurement and the plot geolocation and extent were excluded. Next, the plot data were projected to the geographic reference system WGS-84 and harmonized with the input maps by averaging the biomass values located within the same 1 km pixel. The field plots not fully located within one pixel were attributed to the map cell where the majority of the plot area (i.e., the plot centroid) was located.

Lastly, the representativeness of the plot over the 1km pixels was considered, and the ground data were further screened to discard plots not representative of the map cells in terms of biomass density. More specifically, since the two input maps are not aligned and therefore their pixels do not correspond to the same geographic area, the plot representativeness was assessed on the area of both pixels (identified before the map resampling). The representativeness was evaluated on the basis of the homogeneity of the tree cover and crown size within the pixel, and it was assessed using visual interpretation of high-resolution images provided on the Google Earth platform. If the tree cover and tree crowns were not homogeneous over at least 90% of the pixel area, the plots located within the pixel were discarded. More details on the selection procedure are provided in the Supplementary Information.

Reference biomass maps

The reference biomass maps consisted of high quality local or national maps published in the scientific literature. Maps providing biomass estimates grouped in classes (e.g., Willcock et al., 2012) were not used since the class values represent the mean biomass over large areas, usually spanning multiple strata used in the present study (see 'Stratification approach'). The reference biomass maps were first pre-processed to match the input maps through re-projection, aggregation and resampling using the same procedures described for the pre-processing of the Baccini map. Then, only the cells with largest confidence (i.e., lowest uncertainty) were selected from the maps. Since uncertainty maps were usually not available, and considering that the reference maps were based on empirical models, the map cells with greatest confidence were assumed to be those in correspondence of the training data (field plots and/or LiDAR data). When the locations of the training data were not available, random pixels were extracted from the maps. In order to compile a reference database that was representative of the area of interest and well balanced among the various input datasets (as defined in 'Consolidation of the reference dataset'), the amount of reference data extracted from the biomass maps was proportional to their area and not greater than the amount of samples provided by the field datasets representing a similar area. In the case where maps with extensive training areas provided a disproportionate number of reference pixels, a further screening selected only the areas underpinned by the largest amount of training data.

Selected reference data

The biomass reference dataset compiled for this study consists of 15,969 1-km reference pixels, distributed as follows: 953 in Africa, 449 in South America, 9,167 in Central America, 400 in Asia and 5,000 in Australia (Fig. 2, Table 1). The reference data were relatively uniformly distributed among the strata (Table S5) but their amount varied considerably by continent. The average amount of reference data per stratum ranged from 50 (Asia) to 1,144 (Central America) reference pixels and their variability (computed as standard deviation relative to the mean) ranged from 25% (South America) to 57% (Central America). The uneven distribution of reference data across the continents is mostly caused by the availability of ground observations: in order to have a balanced reference dataset for each stratum, the reference data extracted from biomass maps were limited to the (smaller) amount of direct field observations. When biomass maps were the only source of data this constrain was not occurring and larger datasets could be derived from the maps (i.e., Central America, Australia). Ad example, all pixels (4,263) in correspondence of the training data could be selected from the biomass map of Mexico while only 13% of the 1,167 pixels with training data could be selected from the biomass map of Uganda to maintain comparability with smaller reference datasets available in Africa.

The reference data were selected from 18 ground datasets providing 1,591 research field observations and 5,036 forest inventory plots, and from 9 high resolution biomass maps calibrated by field observations and, in four cases, airborne LiDAR data. The field plots used for the calibration of the maps are not included in this section because they were only used to select the reference pixels from the maps. The visual screening of the field plots removed 35% of the input data (from 6,627 to 4,283) and their aggregation to 1 km resolution further removed 70% of the reference units derived from field plots (from 4,283 to 1,274), while 10,741 reference pixels were extracted from the high-resolution biomass maps. The criteria used to select the reference pixels for each map are reported in Table S3. The consolidation procedure added 3,954 reference data to the final reference dataset that consisted of 15,969 units (Table S2). In particular, ground observations were mostly discarded in areas characterized by fragmented or heterogeneous vegetation cover and high biomass spatial variability. In such contexts, reference data were often acquired from the biomass maps. The reference dataset was compared to the input maps, revealing substantial linear correlation (ranging from 0.60 to 0.77) between the errors of the Saatchi and Baccini maps and RMSE values in the same order of magnitude for all continents, ranging from 96 to 124 Mg ha^{-1}, with the exception of Australia (45 Mg ha^{-1}) (Table S4).

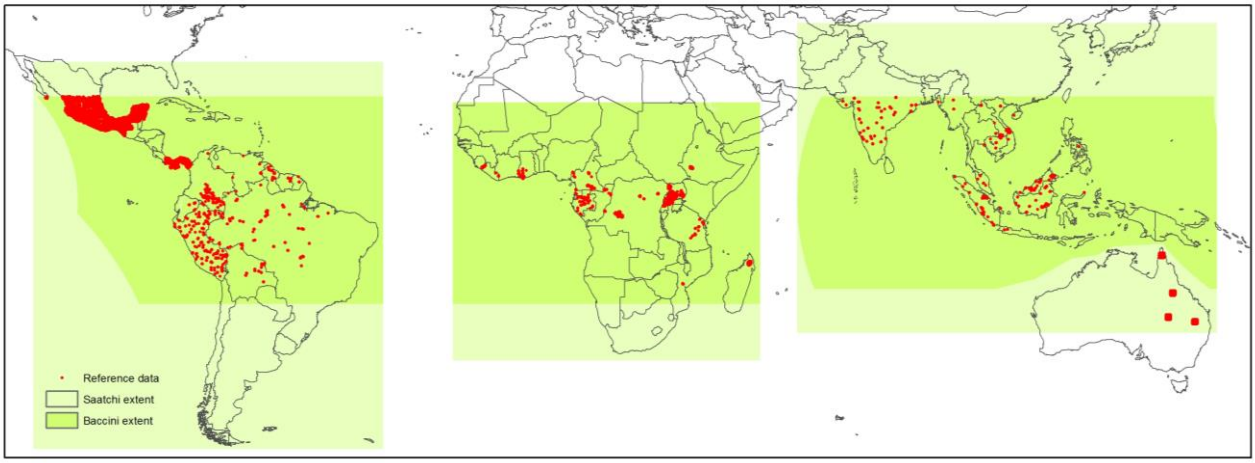

Figure 2: Biomass reference dataset for the tropics and spatial coverage of the two input maps

Table 1: Number of reference data (plots and 1-km pixels) selected after the screening, upscaling and consolidating procedures, per continent. The reference data selected for each individual dataset are reported in Table S2. The field plots underpinning the reference biomass maps are not included.

Continent	Available	Selected		Consolidated
	Plots	*Plots*	*Pixels*	*Pixels*
Africa	2,281	1,976	953	953
S. America	648	474	449	449
C. America	-	-	5,260	9,167
Asia	3,698	1,833	353	400
Australia	-	-	5,000	5,000
Total TROPICS	**6,627**	**4,283**	**12,015**	**16,969**

Modelling approach

The fusion model

The integration of the two input maps was performed with a fusion model based on the concept presented by Ge et al. (2014) and further developed for this study. The fusion model consists of bias removal and weighted linear averaging of the input maps to produce an output with greater accuracy than each of the input maps. The reference biomass dataset described above was used to calibrate the model and to assess the accuracy of the input and fused maps. A specific model was developed for each stratum (see 'Stratification approach').

Following Ge et al. (2014), the *p* input maps for locations $s \in D$, where D is the geographical domain of interest common to the input maps, were combined using a weighted linear average:

$$(1) \quad f(s) = \sum_{i=1}^{p} w_i(s) \cdot (z_i(s) - v_i(s))$$

where *f* is the fused map, the $w_i(s)$ are weights, z_i the estimate of the i-th input map and $v_i(s)$ is the bias estimate. The bias term was computed as the average difference between the input map and the reference data. The weights were obtained from a statistical model that assumes the map estimates z_i to be the sum of the true biomass b_i with a bias term v_i and a random noise term ε_i with zero mean for each location $s \in D$. We further assumed that the ε_i of the input maps are jointly normally distributed with variance-covariance matrix $\boldsymbol{C}(s)$. Differently from Ge et al. (2014), $\boldsymbol{C}(s)$ was estimated using a robust covariance estimator as implemented by the 'robust' package in R (Wang et al., 2014), which uses the Stahel-Donoho estimator for strata with fewer than 5,000 observations and the Fast Minimum Covariance Determinant estimator for larger strata. Under these assumptions, the variance of the estimation error of the fused map $f(s)$ is minimized by calculating the weights $w(s)$ as Searle (1971. p. 89):

$$(2) \quad w(s)^T = \left(\mathbf{1}^T \mathbf{C}(s)^{-1} \mathbf{1}\right)^{-1} \mathbf{1}^T \mathbf{C}(s)^{-1}$$

where $\mathbf{1}=[1, ..., 1]^T$ is the p-dimensional unit vector and where T means transpose. Larger weights were assigned to the map with lower error variance. The fusion model assured that the variance of the error in the fused map was smaller than that of the input maps (Bates and Granger, 1969), especially if the errors associated with these maps were not strongly positively correlated and their error variances were close to the smallest error variance. The fusion model can be applied to any number of input maps. Where there is only one input map, the model estimates and removes its bias and the weights are set equal to 1.

The model parameters

The fusion model computed a set of bias and weight parameters for each stratum and continent on the basis of the respective reference data, and used these for the linear weighted combination of the input maps (Table S5). Since the stratification approach grouped together data with similar error patterns (see 'Stratification approach'), the biases varied considerably among the strata and could reach values up to ±200 Mg ha^{-1}. However, considering the area of the strata, the biases of both

input maps were smaller than ± 45 Mg ha^{-1} for at least 50% of the area of all continents and smaller than ±100 Mg ha^{-1} for 81% - 98% of the area of all continents.

Stratification approach

Error modelling

Preliminary comparison of the reference data with the input maps showed that the error variances and biases of the input maps were not spatially homogeneous but varied considerably in different regions. Since the fusion model is based on bias removal and weighted combination of the input maps, the more homogeneous the error characteristics in the input maps are, the better they can be reduced by the model. For this reason, the stratification approach aimed at identifying areas with homogeneous error structure (hereafter named 'error strata') in both input maps. A first stratification was done by geographic location (namely Central America, South America, Africa, Asia and Australia) to reflect the regional allometric relationships between biomass and tree diameter and height (Feldpausch et al., 2011, 2012). Then, the error strata were identified for each continent, using a two-step process. Firstly, the error maps of the Saatchi and Baccini maps were predicted separately on the basis of their biomass estimates and land cover, tree cover and tree height parameters by using a Random Forest model (Breiman, 2001), calibrated on the basis of the reference dataset. Secondly, the error maps of the Saatchi and Baccini datasets were clustered using the K-Means approach. Eight clusters (hence, eight error strata) was considered as a sensible trade-off between homogeneity of the errors of the input maps and number of reference observations available per stratum (Fig. S1). The performance of this approach was assessed on the basis of the root mean square error (RMSE) of the models that predicted the errors of the input maps. Since the ensemble modelling approach used in this study (Random Forest) includes a certain level of randomness, the model performance was computed as an average of 100 model runs (Fig. S2, Fig. S3). The RMSE computed on the Out-Of-Bag data (i.e., data not used for training) of the Random Forest models for the Baccini extent ranged between 22.8 ± 0.3 Mg ha^{-1} for Central America to 83.7 ± 2.5 Mg ha^{-1} in Africa, with the two models (one for each input map) achieving similar accuracies in each continent (Fig. S2, Fig. S3). In most cases the main predictors of the errors of the input maps were the biomass values of the maps themselves, followed by tree cover and tree height, while land cover was always the least important predictor (Table S1). Further details on error modelling and processing of the input data are provided in the Supplementary Information.

The stratification map identifies eight strata for each continent with homogeneous error patterns in the input maps (Fig. S4). The use of a stratification based on the errors of the input maps was compared with a stratification based on an alternative variable, such as land cover (used by Ge et al., 2014), tree cover or tree height. Each of these variables was aggregated into eight classes to maintain comparability with the number of clusters used in the error strata, and each stratification map was used to develop a specific fused map. The performance of alternative stratification approaches was assessed by validating the respective fused maps. The results (Fig. S5) demonstrated that the stratification based on error modelling and clustering (i.e., the error strata) produced a fused map with higher accuracy than that of the maps based on other stratification approaches, and therefore was used in this study.

Consolidation of the reference dataset

Considering that the parameters of the fusion model (i.e. weight and bias) are sensitive to the characteristics of the reference data, each stratum requires that calibration data are relatively well-balanced between the various reference datasets. Specifically, if a stratum contains few calibration data, the model becomes more sensitive to outliers, while if a reference dataset is much larger than the others, the model is more strongly determined by the dominant dataset. For these reasons, where the reference dataset was under-represented or un-balanced, it was consolidated by additional reference data taken from the reference biomass maps, if available. The reference data were considered insufficient if a stratum had less than half of the average reference data per stratum, and were considered un-balanced if a single dataset provided more than 75% of the reference data of the whole stratum and it was not representative of more than 75% of its area. In such cases, additional reference data were randomly extracted from the reference biomass maps that did not provide more than 75% of the reference data. The amount of data to be extracted from each map was computed in a way to obtain a reference dataset with an average number of reference data per stratum and not dominated by a single dataset. If necessary, additional training data representing areas with no biomass (e.g., bare soil) were included, using visual analysis of Google Earth images to identify locations without vegetation.

Post-processing

Predictions outside the coverage of the Baccini map

The Baccini map covers the tropical belt between 23.4 degree north latitude and 23.4 degree south latitude while the Saatchi map presents a larger latitudinal coverage (Fig. 2). The fusion model was

firstly applied to the area common to both input maps (Baccini extent) and then extended to the area where only the Saatchi map is available. In the latter area, the model focused only on removing the bias of the Saatchi map using the values estimated for the Baccini extent. The model predictions for the Saatchi extent were mosaicked to those for the Baccini extent using a smoothing function (inverse distance weight) on an overlapping area of 1 degree within the Baccini extent between the two maps. The resulting fused map was projected to an equal area reference system (MODIS Sinusoidal) before computing the total biomass stocks for each continent, which were obtained by summing the products of the biomass density of each pixel with their area. Water bodies were masked over the whole study area using the ESA CCI Water Bodies map (ESA, 2014).

Assessing biomass in intact and non-intact forest

The biomass estimates of the fused and input maps in forest areas were further investigated regarding their distribution in ecozones and between intact and non-intact landscapes. Forest areas were defined as areas dominated by tree cover according to the GLC2000 map (classes 1-10 in the global legend of GLC2000). Ecozones were defined according to the Global Ecological Zone (GEZ) map for the year 2000 (FAO, 2000). The intact landscapes were defined according to the Intact Forest Landscape (IFL) map for the year 2000 (Potapov et al., 2008). On the basis of these datasets the mean forest biomass density of the fused and input maps were computed for intact and non-intact landscapes for each continent and major ecozone. To reduce the impact of spatial inaccuracies in the maps only ecozones with intact forest areas larger than 1,000 km^2 were considered. The mean biomass density of intact and non-intact forests per continent was computed as the area-weighted mean of the contributing ecozones.

Validation and uncertainty

Validation was performed by randomly splitting the reference data into a calibration set (70% of the data) and a validation set (remaining 30%). The ‘final’ fused map presented in Fig. 3 used 100% of the reference data and for validation purposes a ‘test’ fused map was produced using only the calibration data and its estimates, as well as those of the input maps, were compared with the validation data. To maintain full independence, validation data were not used for any step related to the development of the fused map, including production of the stratification map. To account for any potential impacts of the random selection of validation data, the procedure was repeated 100 times, computing each time a new random selection of the calibration and validation datasets. This procedure allowed computing the mean RMSE and assessing its standard deviation for each map.

The uncertainty of the fused map was computed with respect to model uncertainty, not including the error sources in the input data (see 'Discussion'). The model uncertainty consisted of the expected variance of the error of the fused map (which is assumed bias-free) and was derived for each stratum from $\boldsymbol{C(s)}$. The error variance was converted to an uncertainty map by reclassifying the stratification map.

Results

Biomass map

The fusion model produced a biomass map at 1 km resolution for the tropical region, with an extent equal to that of the Saatchi map (Fig. 3). In terms of aboveground stocks, the fused map gave biomass estimates lower than both input maps at continental level. The total stock was 451 Pg dry mass, 17% lower than the estimate of the Saatchi map (545 Pg) for the same extent. Considering the same common area (Baccini extent), the fused map estimate was 360 Pg, 13% and 21% lower than the Saatchi (413 Pg) and Baccini (457 Pg) estimates, respectively (Table S6).

Moreover, the fused map presented spatial patterns substantially different from both input maps (Fig. 4): the biomass estimates were higher than both input maps in the dense forest areas in the Congo basin, in West Africa, in the north-eastern part of the Amazon basin (Guyana shield) and in South-East Asia, and lower in Central America and in most dry vegetation areas of Africa. In the central part of the Amazon basin the fused map showed lower estimates than the Baccini map and higher estimates than the Saatchi map, while in the southern part of the Amazon basin these differences were inversed. Similar trends emerged when comparing the maps separately for intact and non-intact forest ecozones (Supporting Information). In addition, the average difference between intact and non-intact forests was larger than that derived from the input maps in Africa, Asia and Australia, similar or slightly larger in South America, and smaller in Central America (Fig. S7).

The fused map records the highest biomass density (> 400 Mg ha^{-1}) in the Guyana shield, in the Central and Western part of the Congo basin and in the intact forest areas of Borneo and Papua New Guinea. The analysis of the distribution of forest biomass in intact and non-intact ecozones showed that, according to the fused map, the mean biomass density was greatest in intact African (360 Mg ha^{-1}) and Asian (328 Mg ha^{-1}) forests, followed by intact forests in South America (262 Mg ha^{-1}),

Asia (202 Mg ha^{-1}), Australia (162 Mg ha^{-1}) and Central America (135 Mg ha^{-1}) (Fig. S7). Biomass in non-intact forests was much lower in all regions (Africa, 76 Mg ha^{-1}; South America, 136 Mg ha^{-1}; Asia, 196 Mg ha^{-1}; Australia, 90 Mg ha^{-1}; and Central America, 46 Mg ha^{-1}).

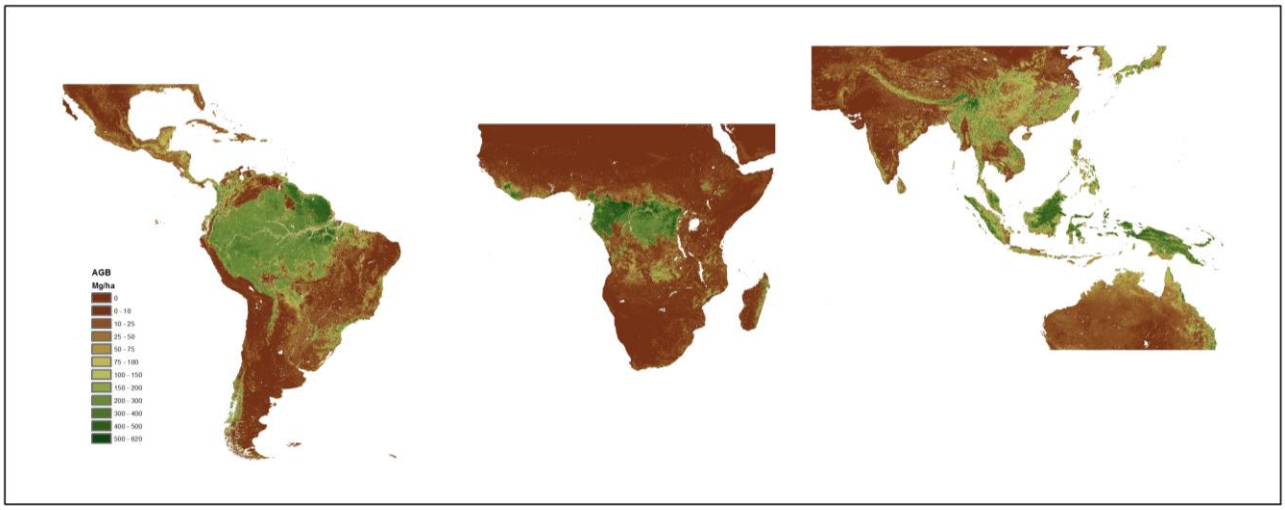

Figure 3: Fused map, representing the distribution of live woody aboveground biomass (AGB) for all land cover types at 1 km resolution for the tropical region.

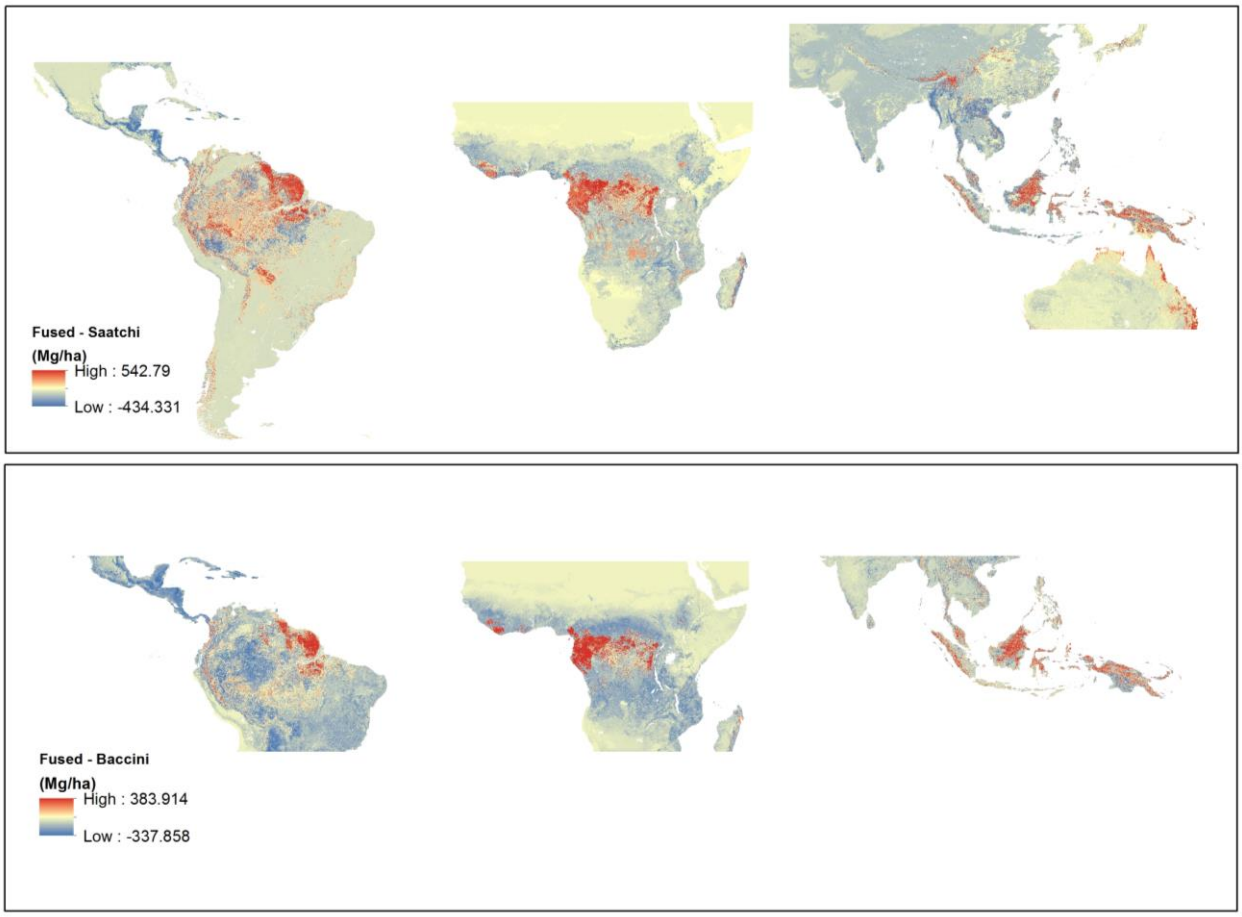

Figure 4: Difference maps obtained by subtracting the fused map from the Saatchi map (top) and the Baccini map (bottom).

Validation

The validation exercise showed that the fused map achieved a lower RMSE (a decrease of 8 – 74%) and bias (a decrease of 90 – 153%) than the input maps for all continents (Fig. 5). While the RMSE of the fused map was consistently lower than that of the input maps but still substantial (87 – 98 Mg ha^{-1}) in the largest continents (Africa, South America and Asia), the mean error (bias) of the fused map was almost null in most cases. Moreover, in the three main continents the bias of the input maps tended to vary with biomass, with overestimation at low values and underestimation at high values, while the errors of the fused map were more consistently distributed (Fig. 6). When computing the error statistics as average of the regional validation results weighted by the respective area coverage, the mean bias (in absolute terms) for the fused, Saatchi and Baccini maps was 5, 21 and 28 Mg ha^{-1} and the mean RMSE was 89, 104 and 112 Mg ha^{-1}, respectively (Fig. 5).

The accuracy of the input maps was computed using the validation dataset (30% of the reference dataset) to be consistent with the accuracy of the fused map. The accuracy of the input maps was

also computed using all reference data and the results (Table S4) were similar to those based on the validation dataset.

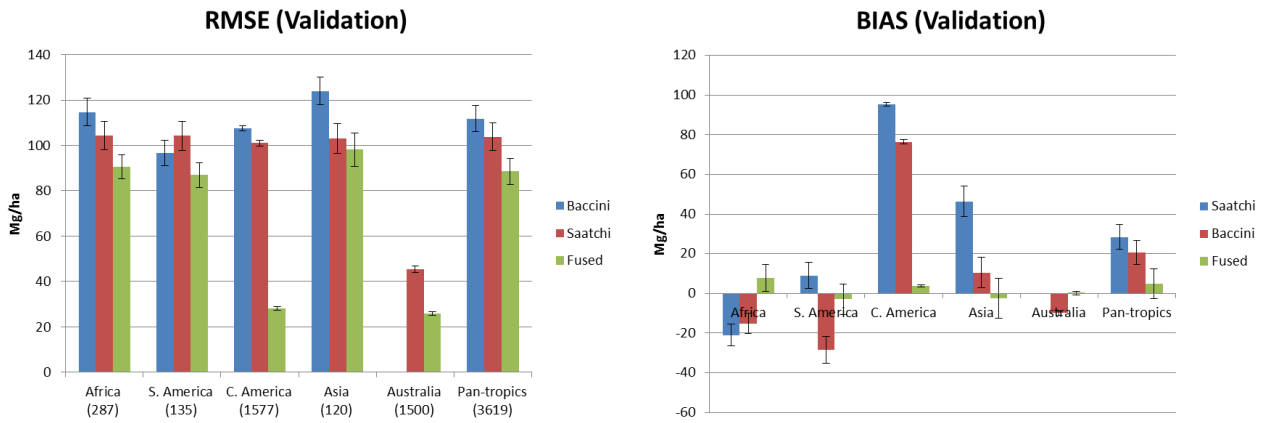

Figure 5: RMSE (left) and bias (right) of the fused and input maps (in Mg ha^{-1}) per continent obtained using independent reference data not used for model development. The error bars indicate one standard deviation of the 100 simulations. Numbers reported in brackets indicate the number of reference observations used for each continent.

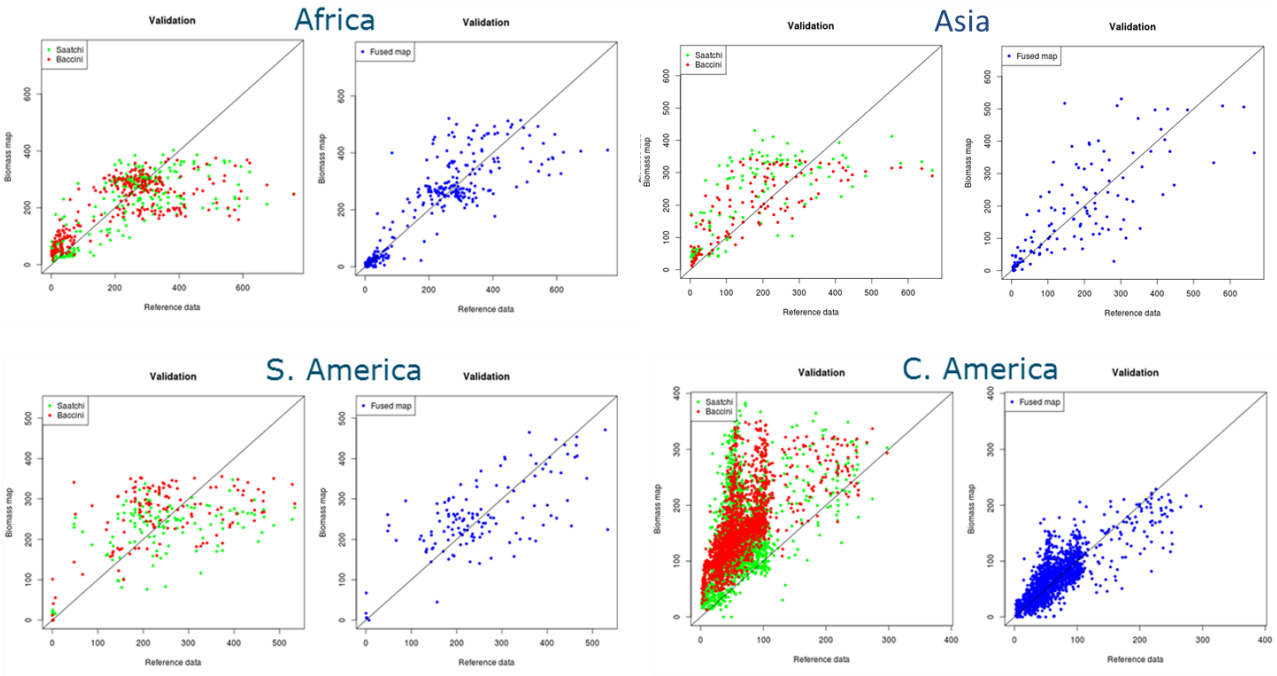

Figure 6: scatterplots of the validation reference data (x-axis) and predictions (y-axis) of the input maps (left plots) and fused map (right plots) by continent.

Uncertainty map

The uncertainty of the model predictions at 1 km resolution indicated that the standard deviation of the error of the fused map for each stratum was in the range 11 - 78 Mg ha^{-1}, with largest uncertainties in areas with largest biomass estimates (Congo basin and Eastern Amazon basin). When computed in relative terms (as percentage of the biomass estimate) the model uncertainties presented opposite patterns, with uncertainties larger than the estimates (> 100%) in low biomass areas (< 20 Mg ha^{-1} on average) of Africa, South America and Central America, while high biomass forests (> 210 Mg ha^{-1} on average) had uncertainties lower than 25% (Fig. 7). The uncertainty measure derived from ***C(s)*** is computed only when two or more input maps are available. Hence it could not be calculated for Australia because the model for this continent was based on only one input map (Saatchi map).

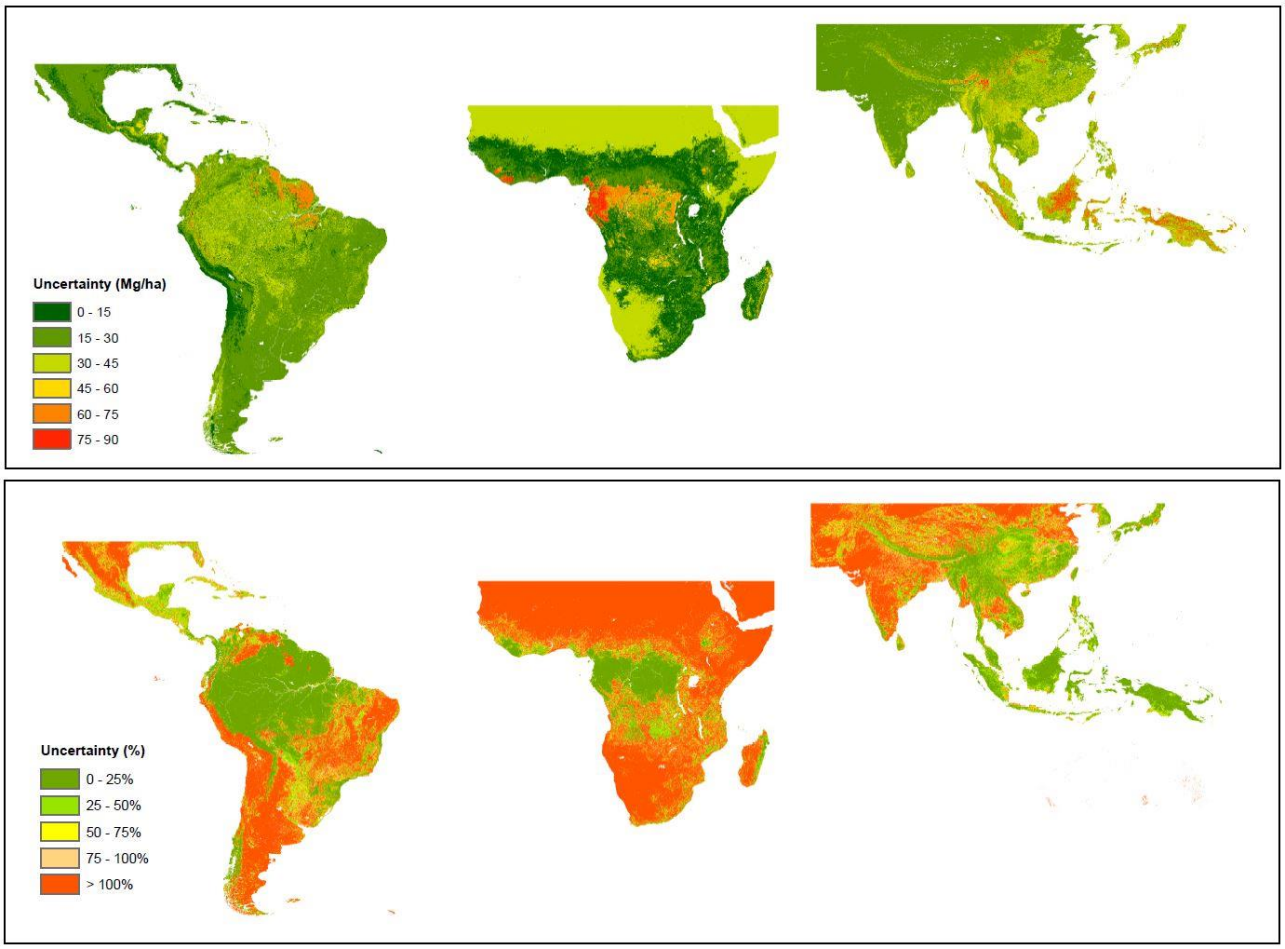

Figure 7: Uncertainty of the fused map, in absolute values (top) and relative to the biomass estimates (bottom), representing one standard deviation of the error of the fused map.

Discussion

Biomass patterns and stocks emerging from the reference data

The biomass map produced with the fusion approach is largely driven by the reference dataset and essentially the method is aimed at spatializing the biomass patterns indicated by the reference data using the support of the input maps. For this reason, great care was taken in the pre-processing of the reference data, which included a two-step quality screening based on metadata analysis and visual interpretation, and their consolidation after stratification. As a result, the reference dataset provides an unprecedented compilation of biomass estimates at 1 km resolution for the tropical region, covering a wide range of vegetation types, biomass ranges and ecological regions across the tropics. It includes the most comprehensive and accurate tropical field plot networks and high quality maps calibrated with airborne LiDAR, which provide more accurate estimates compared to those obtained from other sensors (Zolkos et al., 2013). The main trends present in the fused map emerged from the combination of different and independent reference datasets and are in agreement with the estimates derived from long-term research plot networks (Malhi et al., 2006; Phillips et al. 2009; Lewis et al. 2009; Slik et al., 2010, 2013; Lewis et al., 2013) and high-resolution maps (Asner et al., 2012a, 2012b, 2013, 2014a). Specifically, the biomass patterns in South America represent spatial trends described by research plot networks in the dense intact and non-intact forests in the Amazon basin, forest inventory plots collected in the dense forests of Guyana and samples extracted from biomass maps for Colombia and Peru representing a wide range of vegetation types, from arid grasslands to humid forests. Similarly, biomass patterns depicted in Africa were derived from a combination of various research plots in dense undisturbed forest (Gabon, Cameroon, Democratic Republic of Congo, Ghana, Liberia), inventory plots in forest concessions (Democratic Republic of Congo), biomass maps in woodland and savannah ecosystems (Uganda, Mozambique) and research plots and maps in montane forests (Ethiopia, Madagascar). Most vegetation types in Central America, Asia and Australia were also well-represented by the extensive forest inventory plots (Indonesia, Vietnam and Laos) and high-resolution maps (Mexico, Panama, Australia).

In spite of the extensive coverage, the current database is far from being representative of the biomass variability across the tropics. As a consequence, the model estimates are expected to be less accurate in contexts not adequately represented. In the case of the fusion approach, this corresponds to the areas where the input maps present error patterns different than those identified in areas with reference data: in such areas the model parameters used to correct the input maps (bias and weight) may not adequately reflect the errors of the input maps and hence cannot optimally

correct them. In particular, deciduous vegetation and heavily disturbed forest of Africa and South America, and large parts of Asia were lacking quality reference data. Moreover, even though plot data were spatially distributed over the central Amazon and the Congo basin, large extents of these two main blocks of tropical forest have never been measured (cf. maps in Mitchard et al. 2014; Lewis et al. 2013). Considering the evidence of significant local differences in forest structure and biomass density within the same forest ecosystems (Kearsley et al., 2013), additional data are needed to strengthen the confidence of the fused map as well as that of any other biomass map covering the tropical region. Moreover, a dedicated gap analysis to assess the main regions lacking biomass reference data and identify priority areas for new field sampling and LiDAR campaigns would be very valuable for future improved biomass mapping.

Regarding the biomass stocks, a previous study showed that despite their often very strong local differences the two input maps tended to provide similar estimates of total stocks at national and biome scales and presented an overall net difference of 10% for the pan-tropics (Mitchard et al., 2013). However, such convergence is mostly due to compensation of contrasting estimates when averaging over large areas. The larger differences with the estimates of the present study (13% and 21%) suggest an overestimation of the total stocks by the input maps. This is in agreement with the results of two previous studies that, on the basis of reference maps obtained by field-calibrated airborne LiDAR data, identified an overestimation of 23% - 42% of total stocks in the Saatchi and Baccini maps in the Colombian Amazon (Mitchard et al., 2013) and a mean overestimation of about 100 Mg ha^{-1} for the Baccini map in the Colombian and Peruvian Amazon (Baccini and Asner, 2013).

In general, the biomass density values of the fused map were calibrated and therefore in agreement with the existing estimates obtained from plot networks and high resolution maps. The comparison of mean biomass values in intact and non-intact forests stratified by ecozone provided further information on the differences among the maps. The mean biomass values of the fused map in non-intact forests were mostly lower than those of the input maps, suggesting that in disturbed forests the biomass estimates derived from stand height parameters retrieved by spaceborne LiDAR (as in the input maps) tend to be higher compared to those based on tree parameters or very high resolution airborne LiDAR measurements (as in the fused map and reference data). This difference occurred especially in Africa, Asia and Central America while it was less evident in South America and Australia. By contrast, the differences among the maps for intact forests varied by continent, with the fused map having, on average, higher mean biomass values in Africa, Asia and Australia,

lower values in Central America, and variable trends within South America, reflecting the different allometric relationships used by the various datasets in different continents.

As mentioned above, a larger amount of reference data, ideally acquired based on a clear statistical sampling design, instead of an opportunistic one, will be required to confirm such conclusions. While dense sampling of tropical forests using field observations is often impractical, new approaches combining sufficient ground observations of individual trees at calibration plots with airborne LiDAR measurements for larger sampling transects would allow a major increase in the quantity of calibration data. In combination with wall-to-wall medium resolution satellite data (e.g., Landsat) these may be capable of achieving high accuracy over large areas (10% - 20% uncertainty at 1-ha scale) while being cost-effective (e.g., Asner et al. 2014b; Asner et al., 2013). In addition, new technologies, such as terrestrial LiDAR scanning, allows for better estimates at ground level (Calders et al., 2015), reducing considerably the uncertainties of field estimates based on generalized allometric equations without employing destructive sampling. Nevertheless, such techniques benefit from extensive and precise measurements of tree identity in order to determine wood density patterns, since floristic composition influences biomass at multiple scales (e.g., the strong pan-Amazon gradient in wood density shown by ter Steege et al., 2006), and cannot account for variations in hollow stems and rottenness (Nogueira et al., 2006).

Additional error sources

Apart from the uncertainty of the fusion model described above (see 'Uncertainty'), three other sources of error were identified and assessed in the present approach: i) errors in the reference dataset; ii) errors due to temporal mismatch between the reference data and the input maps; iii) errors in the stratification map.

Errors in the reference dataset

The reference dataset is not error-free but it inherits the errors present in the field data and local maps and introduces additional uncertainties during the pre-processing of the data by resampling the maps and by upscaling the plot data to 1 km resolution. In particular, while the geolocation error of the original datasets was considered relatively small (< 50 m) since plot coordinates were collected using GPS measurements and the biomass maps were based on satellite data with accurate geolocation (i.e., Landsat, ALOS, MODIS), larger errors (up to 500 m, half a pixel) could have been introduced with the resampling of the 1 km input maps. All these error sources were

minimized by selecting only the datasets that fulfilled certain quality criteria and by further screening them by visual analysis of high-resolution images available on the Google Earth platform, discarding the data not representative of the respective map pixels. In case of reference data that clearly did not match with the high-resolution images and/or with the input maps (e.g., reporting no biomass in dense forest areas or high biomass on bare land), the data were considered as an error in the reference dataset, a geolocation error in the plots or maps, or it was assumed that a land change process occurred between the plot measurement and the image acquisition time (see next paragraph).

Errors due to temporal mismatch

The temporal difference of input and reference data introduced some uncertainty in the fusion model. The input maps refer to the years 2000 - 2001 (Saatchi) and 2007 - 2008 (Baccini) while the reference data mostly spanned the period 2000 – 2013. Therefore, the differences between the input maps and the reference data may also be due to a temporal mismatch of the datasets. However, changes due to deforestation were most likely excluded during the visual selection of the reference data, when high-resolution images showed clear land changes (e.g., bare land or agriculture) in areas where the input maps provided biomass estimates relative to forest areas (or vice-versa, depending on the timing of acquisition of the datasets). However, changes due to forest regrowth and forest degradation events that did not affect the forest canopy could not be considered with the visual analysis and may have affected the mismatch observed between the reference data and the input maps (< |56 - 78| Mg ha^{-1} for 50% of the cases of the Saatchi and Baccini maps, respectively). The mismatch was in the range of biomass changes due to regrowth (1 - 13 Mg ha^{-1} $year^{-1}$) (IPCC, 2003) or low-intensity degradation (14 - 100 Mg ha^{-1}, or 3-15% of total stock) (Pearson et al., 2014; Asner et al., 2010). On the other hand, considering the area affected by degradation (about 20% in the humid tropics) (Asner et al., 2009), the temporal mismatch was considered responsible only for a limited part of the large differences observed between the reference data and the input maps. Small additional offsets may also be caused by the documented secular changes in biomass density within intact tropical forests, which has been increasing by 0.2 – 0.5% per year (Phillips et al. 1998, Chave et al. 2008, Phillips and Lewis 2014). It should also be noted that the reference data were used to optimally integrate the input maps, and in the case of a temporal difference the fused map was also 'actualized' to the state of the vegetation when the reference data were acquired. Therefore the fused map cannot be attributed to a specific year and it represents the first decade of the 2000's.

Errors in the stratification map

The errors in the stratification map (i.e., related to the prediction of the errors of the input maps) were still substantial in some areas and affected the fused map in two ways. First, the reference data that were erroneously attributed to a certain stratum introduced 'noise' in the estimation of the model parameters (bias and weight), but the impact of these 'outliers' was largely reduced by the use of a robust covariance estimator. Second, erroneous predictions of the strata caused the use of incorrect model parameters in the combination of the input maps. The latter is considered to be the main source of error of the fused map and indicates that the method can achieve improved results if the errors of the input maps can be predicted more accurately. However, additional analysis showed that, on average, fused maps based on alternative stratification approaches achieved lower accuracy than the map based on an error stratification approach (Fig. S5). Therefore, this approach was preferred over a stratification based on an individual biophysical variable (e.g., tree cover, tree height, land cover or ecozone).

Application of the method at national scale

The fusion method presented in this study allows for the optimal integration of any number of input maps to match the patterns indicated by the reference data. However, the accuracy of the fused map depends on the availability of reference data representative of the error patterns of the input maps. While the current reference database does not represent adequately all error strata for the tropical region, and the model estimates are expected to have lower confidence in under-represented areas, the proposed method may be applied locally and provide improved biomass estimates where additional reference data are available. For example, the fusion method may be applied at national level using existing forest inventory data, research plots and local maps that cover only part of the country to calibrate global or regional maps, which provide national coverage but may not be tailored to the country context. Such country-calibrated biomass maps may be used to support natural resource management and national reporting under the REDD+ mechanism, especially for countries that have limited capacities to map biomass from remote sensing data (Romijn et al. 2012). Considering the increasing number of global or regional biomass datasets based on different data and methodologies expected in the coming years, and that likely there will not be a single 'best map' but rather the accuracy of each will vary spatially, the fusion approach may allow to optimally combine and adjust available datasets to local biomass patterns identified by reference data.

Acknowledgments

This study was supported by the EU GEOCARON project. Data were also acquired by the Sustainable Landscapes Brazil project supported by the Brazilian Agricultural Research Corporation (EMBRAPA), the US Forest Service, and USAID, and the US Department of State. OP, SLL and LQ acknowledge the support of the European Research Council (T-FORCES), SLL and TS were supported by CIFOR/USAID; SLL was also supported by a Philip Leverhulme Prize.

References

Asner GP, Clark JK, Mascaro J et al. (2012) High-resolution mapping of forest carbon stocks in the Colombian Amazon. *Biogeosciences*, **9**, 2683–2696.

Asner GP, Clark JK, Mascaro J et al. (2012) Human and environmental controls over aboveground carbon storage in Madagascar. *Carbon Balance and Management*, **7**, 2.

Asner GP, Mascaro J, Anderson C et al. (2013) High-fidelity national carbon mapping for resource management and REDD+. *Carbon balance and management*, **8**, 7.

Asner GP, Mascaro J (2014) Mapping tropical forest carbon: Calibrating plot estimates to a simple LiDAR metric. *Remote Sensing of Environment*, **140**, 614–624.

Asner GP, Knapp DE, Martin RE et al. (2014) Targeted carbon conservation at national scales with high-resolution monitoring. *Proceedings of the National Academy of Sciences*, **111**, E5016–E5022.

Avitabile V, Herold M, Henry M, Schmullius C (2011) Mapping biomass with remote sensing: a comparison of methods for the case study of Uganda. *Carbon Balance and Management*, **6**, 7.

Avitabile V, Baccini A, Friedl M a., Schmullius C (2012) Capabilities and limitations of Landsat and land cover data for aboveground woody biomass estimation of Uganda. *Remote Sensing of Environment*, **117**, 366–380.

Baccini a., Goetz SJ, Walker WS et al. (2012) Estimated carbon dioxide emissions from tropical deforestation improved by carbon-density maps. *Nature Climate Change*, **2**, 182–185.

Baccini A, Asner GP (2013) Improving pantropical forest carbon maps with airborne LiDAR sampling. *Carbon Management*, **4**, 591–600.

Bates JM, Granger CWJ (1969) The Combination of Forecasts. *Journal of the Operational Research Society*, **20**, 451–468.

Birdsey R, Angeles-Perez G, Kurz W a et al. (2013) Approaches to monitoring changes in carbon stocks for REDD+. *Carbon Management*, **4**, 519–537.

Breiman L (2001) Random forests. *Machine Learning*, **45**, 5−23.

Calders K, Newnham G, Burt A et al. (2015) Nondestructive estimates of above-ground biomass using terrestrial laser scanning. *Methods in Ecology and Evolution*, **6**, 198–208.

Cartus O, Kellndorfer J, Walker W, Franco C, Bishop J, Santos L, Michel-Fuentes JM (2014) A National, Detailed Map of Forest Aboveground Carbon Stocks in Mexico. *Remote Sensing*, **6**, 5559–5588.

Chave J, Olivier J, Bongers F et al. (2008) Above-ground biomass and productivity in a rain forest of eastern South America. *Journal of Tropical Ecology*, **24**, 355–366.

ESA, 2014. Global Water Bodies. http://www.esa-landcover-cci.org/

FAO, 2000. Global ecological zoning for the global forest resources assessment 2000. FAO FRA Working Paper Rome, Italy; 2001

Feldpausch TR, Banin L, Phillips OL et al. (2011) Height-diameter allometry of tropical forest trees. *Biogeosciences*, **8**, 1081–1106.

Feldpausch TR, Lloyd J, Lewis SL et al. (2012) Tree height integrated into pantropical forest biomass estimates. *Biogeosciences*, **9**, 3381–3403.

Ge Y, Avitabile V, Heuvelink GBM, Wang J, Herold M (2014) Fusion of pan-tropical biomass maps using weighted averaging and regional calibration data. *International Journal of Applied Earth Observation and Geoinformation*, **31**, 13–24.

Goetz S, Dubayah R (2011) Advances in remote sensing technology and implications for measuring and monitoring forest carbon stocks and change. *Carbon Management*, **2**, 231–244.

Grace J, Mitchard E, Gloor E (2014) Perturbations in the carbon budget of the tropics. *Global Change Biology*.

Harris NL, Brown S, Hagen SC et al. (2012) Baseline Map of Carbon Emissions from Deforestation in Tropical Regions. *Science*, **336**, 1573–1576.

Houghton RA, House JI, Pongratz J et al. (2012) Carbon emissions from land use and land-cover change. *Biogeosciences*, **9**, 5125–5142.

Jiahui W, Zamar R, Marazzi A, et al. (2014). robust: Robust Library. R package version 0.4-16. http://CRAN.R-project.org/package=robust.

Kearsley E, de Haulleville T, Hufkens K et al. (2013) Conventional tree height-diameter relationships significantly overestimate aboveground carbon stocks in the Central Congo Basin. *Nature communications*, **4**, 2269.

IPCC (2003). Good practice guidance for land use, land-use change and forestry. IPCC National Greenhouse Gas Inventories Programme, Technical Support Unit. Hayama, Japan: Institute for Global Environmental Strategies.

Langner A, Achard F, Grassi G (2014) Can recent pan-tropical biomass maps be used to derive alternative Tier 1 values for reporting REDD+ activities under UNFCCC? *Environmental Research Letters*, **9**, 124008.

Lewis SL, Sonké B, Sunderland T et al. (2013) Above-ground biomass and structure of 260 African tropical forests. *Philosophical transactions of the Royal Society of London. Series B, Biological sciences*, **368**, 20120295.

Lewis SL, Lopez-Gonzalez G, Sonké B et al. (2009) Increasing carbon storage in intact African tropical forests. *Nature*, **457**, 1003–1006.

Malhi Y, Wood D, Baker TR et al. (2006) The regional variation of aboveground live biomass in old-growth Amazonian forests. *Global Change Biology*, **12**, 1107–1138.

Mitchard ET, Saatchi SS, Baccini A, Asner GP, Goetz SJ, Harris NL, Brown S (2013) Uncertainty in the spatial distribution of tropical forest biomass: a comparison of pan-tropical maps. *Carbon balance and management*, **8**, 10.

Mitchard ET a, Feldpausch TR, Brienen RJW et al. (2014) Markedly divergent estimates of Amazon forest carbon density from ground plots and satellites. *Global Ecology and Biogeography*, **23**, 935–946.

Nogueira MA, Diaz G, Andrioli W, Falconi F a., Stangarlin JR (2006) Secondary metabolites from Diplodia maydis and Sclerotium rolfsii with antibiotic activity. *Brazilian Journal of Microbiology*, **37**, 14–16.

Pearson TRH, Brown S, Casarim FM (2014) Carbon emissions from tropical forest degradation caused by logging. *Environmental Research Letters*, **034017**, 11.

Phillips, O. L., Malhi, Y., Higuchi, N., Laurance, W., Nuñez, P., Vásquez, R., Laurance, S., Ferreira, L., Stern, M., Brown, S., Grace J (1998) Changes in the carbon balance of Tropical Forests: Evidence from long-term plots. *Science*, **282**, 439–442.

Phillips OL, Aragão LEOC, Lewis SL et al. (2009) Drought sensitivity of the Amazon Rainforest. *Science*, **323**, 1344–1347.

Phillips OL, Lewis SL (2014) Evaluating the tropical forest carbon sink. *Global Change Biology*, **20**, 2039–2041.

Potapov P, Yaroshenko A, Turubanova S et al. (2008) Mapping the world's intact forest landscapes by remote sensing. *Ecology and Society*, **13**.

Romijn E, Herold M, Kooistra L, Murdiyarso D, Verchot L (2012) Assessing capacities of non-Annex I countries for national forest monitoring in the context of REDD+. *Environmental Science and Policy*, **19-20**, 33–48.

Saatchi SS, Harris NL, Brown S et al. (2011) Benchmark map of forest carbon stocks in tropical regions across three continents. *Proceedings of the National Academy of Sciences*, 108, 9899–9904.

Saatchi SS, Mascaro J, Xu L et al. (2014) Seeing the forest beyond the trees. *Global Ecology & Biogeography*, **23**, 935 – 946.

Searle SR (1971) *Linear Models*, Vol. XXI. WILEY-VCH Verlag, York-London-Sydney-Toronto, 532 pp.

Slik JWF, Paoli G, Mcguire K et al. (2013) Large trees drive forest aboveground biomass variation in moist lowland forests across the tropics. *Global Ecology and Biogeography*, **22**, 1261–1271.

Ter Steege H, Pitman NC a, Phillips OL et al. (2006) Continental-scale patterns of canopy tree composition and function across Amazonia. *Nature*, **443**, 444–447.

Willcock S, Phillips OL, Platts PJ et al. (2012) Towards Regional, Error-Bounded Landscape Carbon Storage Estimates for Data-Deficient Areas of the World. *PLoS ONE*, **7**, 1–10.

Wright JS (2013) The carbon sink in intact tropical forests. *Global Change Biology*, **19**, 337–339.

Ziegler AD, Phelps J, Yuen JQ et al. (2012) Carbon outcomes of major land-cover transitions in SE Asia: Great uncertainties and REDD+ policy implications. *Global Change Biology*, **18**, 3087–3099.

Zolkos SG, Goetz SJ, Dubayah R (2013) A meta-analysis of terrestrial aboveground biomass estimation using lidar remote sensing. *Remote Sensing of Environment*, **128**, 289–298.

Supporting Information

Appendix S1. Supplementary methods and results

Appendix S1

Supplementary methods and results

Stratification approach

Error modelling

The stratification approach implemented in this study aimed to identify areas with homogeneous error structure in both input maps. The error maps of the Saatchi and Baccini maps were first predicted separately and then combined in eight error strata per continent using a clustering approach. Since the biomass estimates of the input maps were mostly based on optical and LiDAR data that are sensitive to tree cover and tree height, it was assumed that their uncertainties were related to the spatial variability of these parameters. In addition, the errors of the input maps resulted to be linearly correlated with the respective biomass estimates. For these reasons, the biomass maps themselves as well as global datasets of land cover, tree cover and tree height were used to predict the map errors using a Random Forest model (Breiman, 2001), calibrated on the basis of the reference dataset. Then, the error maps of the Saatchi and Baccini datasets were clustered using the K-Means approach. The number of clusters was determined as a trade-off between homogeneity of the errors of the input maps (quantified as variance (sum of squares) within groups of the error maps) and number of reference observations available per stratum. Eight clusters was considered as a sensible compromise between these two parameters, with a larger number of clusters providing only a marginal increase in homogeneity but leading to a small number of reference data in some strata (Fig. S1). The resulting stratification map presented missing values where the predictors presented no data, i.e. areas without coverage of the Baccini map, or for classes of the categorical predictor (i.e., land cover) without reference data. The missing values were estimated using an additional Random Forest model that predicted the strata (instead of the errors of the input maps) based on 10,000 randomly selected training data. These 'secondary' training data were extracted from the stratification map and included only the predictors without missing values (i.e., Saatchi map, tree cover and tree height). The performance of this approach was assessed on the basis of the RMSE of the models that predicted the errors of the input maps, and on the error rate of the models that predicted the strata for the areas with missing values (Fig. S2, Fig. S3). The performance statistics were computed as an average of 100 model repetitions to account for a certain level of randomness inherent in the ensemble modelling approach used in this study (Random Forest). The importance of the predictor variables was assessed on the basis of the total increase in node purities (measured by residual sum of squares) from splitting on the variable,

averaged over all trees (Liaw and Wiener, 2002) (Table S1). According to this variable, the main predictors of the errors of the input maps were in most cases the biomass values of the maps themselves, followed by tree cover and tree height, while land cover was always the least important predictor.

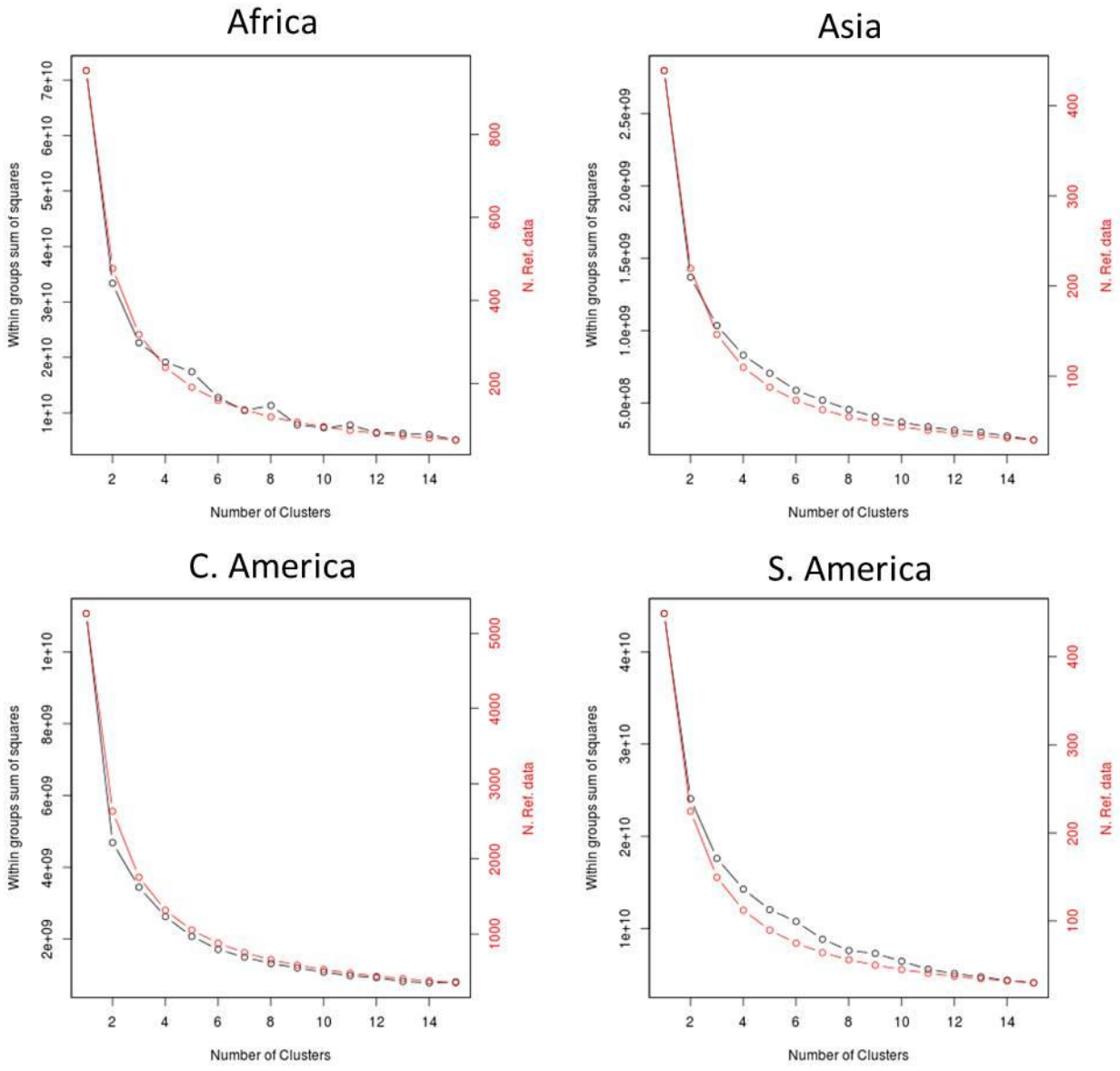

Figure S1: Relation between the number of clusters (x axis), the average number of reference data per cluster (red line) and their homogeneity (within groups sum of square) (black line) when the error maps of the Saatchi and Baccini datasets are clustered using the K-Means approach.

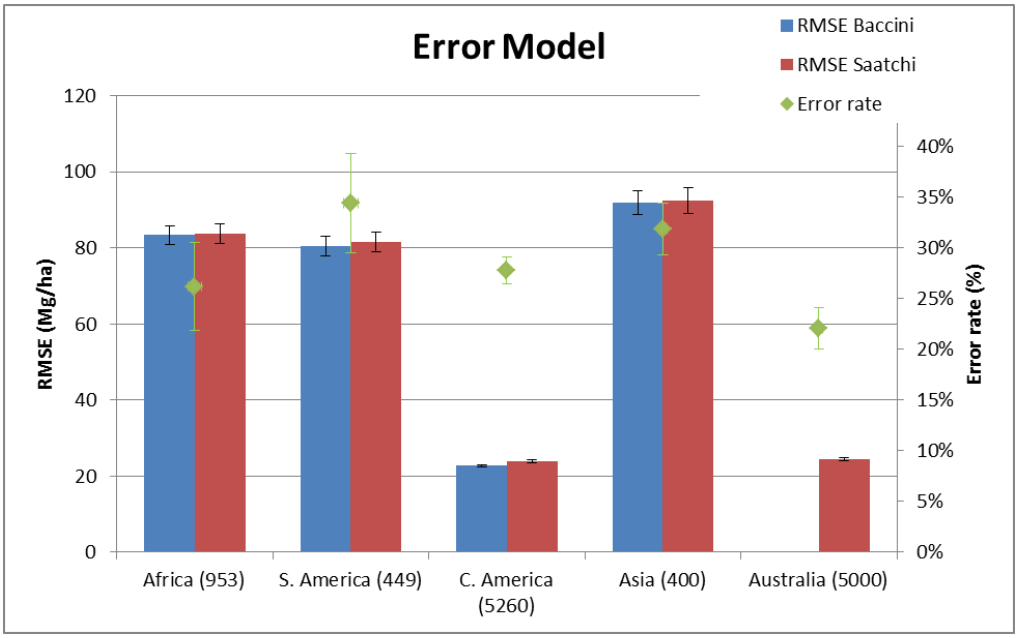

Figure S2: Performance of the models that predicted the error of the input maps (RMSE) and of the models that predicted the strata for the areas not covered by the Baccini map (Error rate). Error statistics are computed as mean of 100 random model repetitions, with the error bars indicating 1 standard deviation.

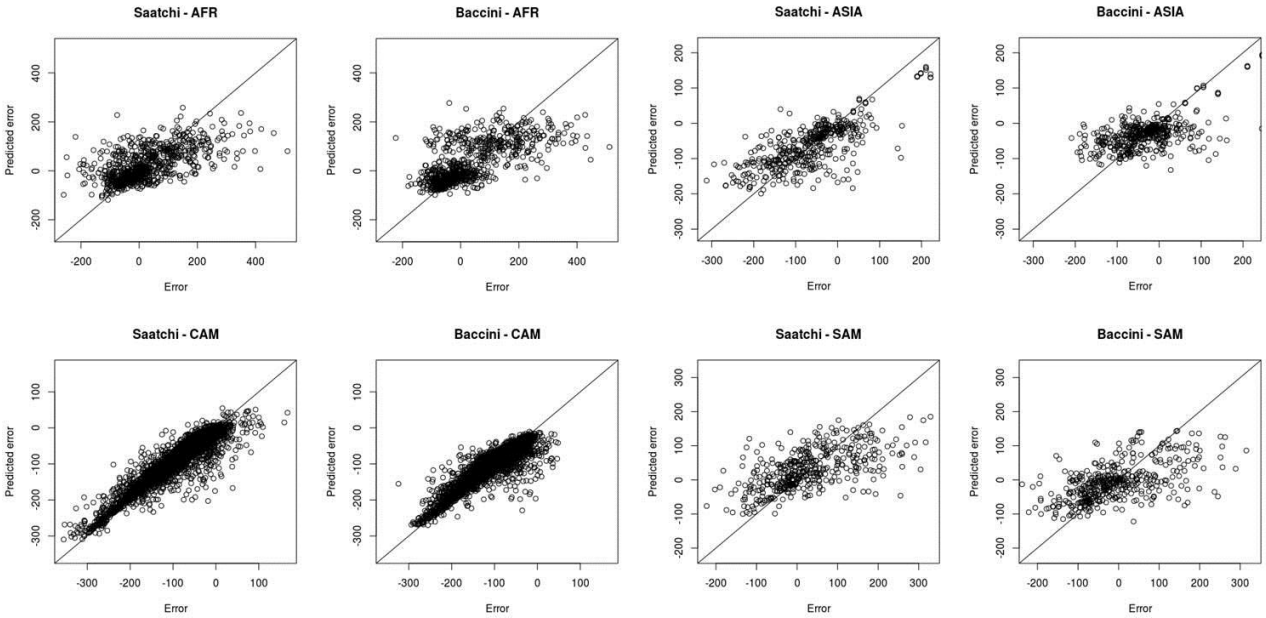

Figure S3: Comparison of predicted errors on the Out-Of-Bag data (i.e., data not used for training the model) with observed errors of the Random Forest models that estimated the errors of the input maps.

Table S1: Importance of the variables used to predict the errors of the input maps by the Random Forest models. The importance is represented by the increase in node purity (x 1000). The variables are the biomass of Saatchi

map ("AGB Saatchi"), biomass of the Baccini map ("AGB Baccini"), forest height ("Height"), tree cover ("VCF") and land cover according to the ESA CCI map ("CCI").

	Africa		S. America		C. America		Asia		Australia
	Saatchi	Baccini	Saatchi	Baccini	Saatchi	Baccini	Saatchi	Baccini	Saatchi
AGB Saatchi	2,607	2,963	1,321	839	14,684	963	1,293	618	1,536
AGB Baccini	2,365	2,737	839	923	1,832	6,219	890	766	-
VCF	2,346	3,223	1,170	1,237	2,469	3,071	614	534	4,971
Height	1,629	1,710	784	748	3,320	1,990	586	537	949
CCI	471	937	22	12	433	239	164	104	1,702

Pre-processing of covariate maps

The maps used to predict the error strata were obtained as follows. The land cover information was derived from the ESA CCI 2005 Land Cover map (ESA, 2014) by first reclassifying it into eight classes representing the main vegetation types (Evergreen forest, Deciduous forest, Woodland, Mosaic Vegetation, Shrubland, Grassland, Cropland, Other land) and then resampling it from its original resolution (330 m) to the resolution of the Saatchi map (1 km) on the basis of the majority criterion. The tree cover value was obtained from the annual MODIS VCF tree cover composites at 250m for the years 2000 – 2010 (DiMiceli et al., 2011). The eleven annual datasets were averaged to a mean decadal composite, spatially aggregated to 1 km resolution and warped to the geographic projection and grid of the Saatchi map (WGS-84). Tree height was directly derived from the Global 3D Vegetation Height map at 1km resolution (Simard et al., 2011). Additional potential land cover and ecosystem predictors, namely the GLC2000 map (Mayaux et al., 2004), the Synmap map (Jung et al., 2006) and the Global Ecological Zone (GEZ) map (FAO, 2000), were tested but discarded after preliminary analysis because they did not provide additional explanatory power to the error models. All maps were resampled to match the grid of the Saatchi map using the nearest neighbor method.

Stratification map and alternative approaches

The stratification map obtained with the approach described above identified eight strata depicting homogeneous error patterns of the input maps for each continent (Central America, South America, Africa, Asia and Australia). The map, reported in Figure S4, was used to identify the parameters (bias and weights) of the fusion model.

Alternative stratification approaches using individual datasets to predict the errors of the input maps, namely land cover, tree cover or tree height, were tested and their performance assessed by validating the respective fused maps. The fused maps based on each stratification map were trained using a calibration dataset (random selection of 70% of the reference data) and compared with the validation dataset (remaining 30% of the reference data) to compute the respective RMSE. To account for any potential impacts of the random selection of validation data, the procedure was repeated 100 times, computing each time a new random selection of the calibration and validation datasets. This procedure allowed to compute the mean RMSE and assess its standard deviation for each map.

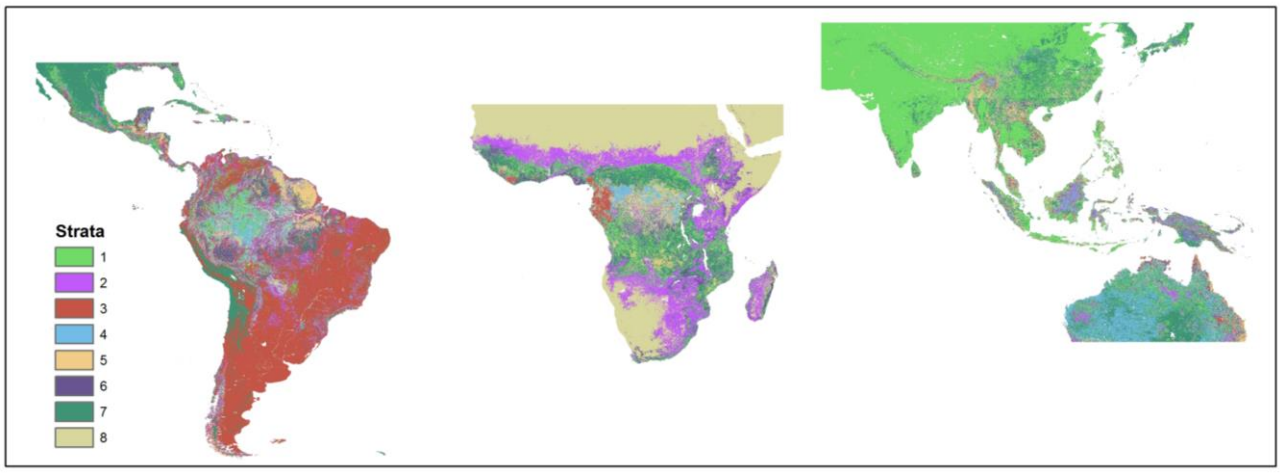

Figure S4: Stratification map, depicting eight strata per continent with homogeneous error patterns of the input maps.

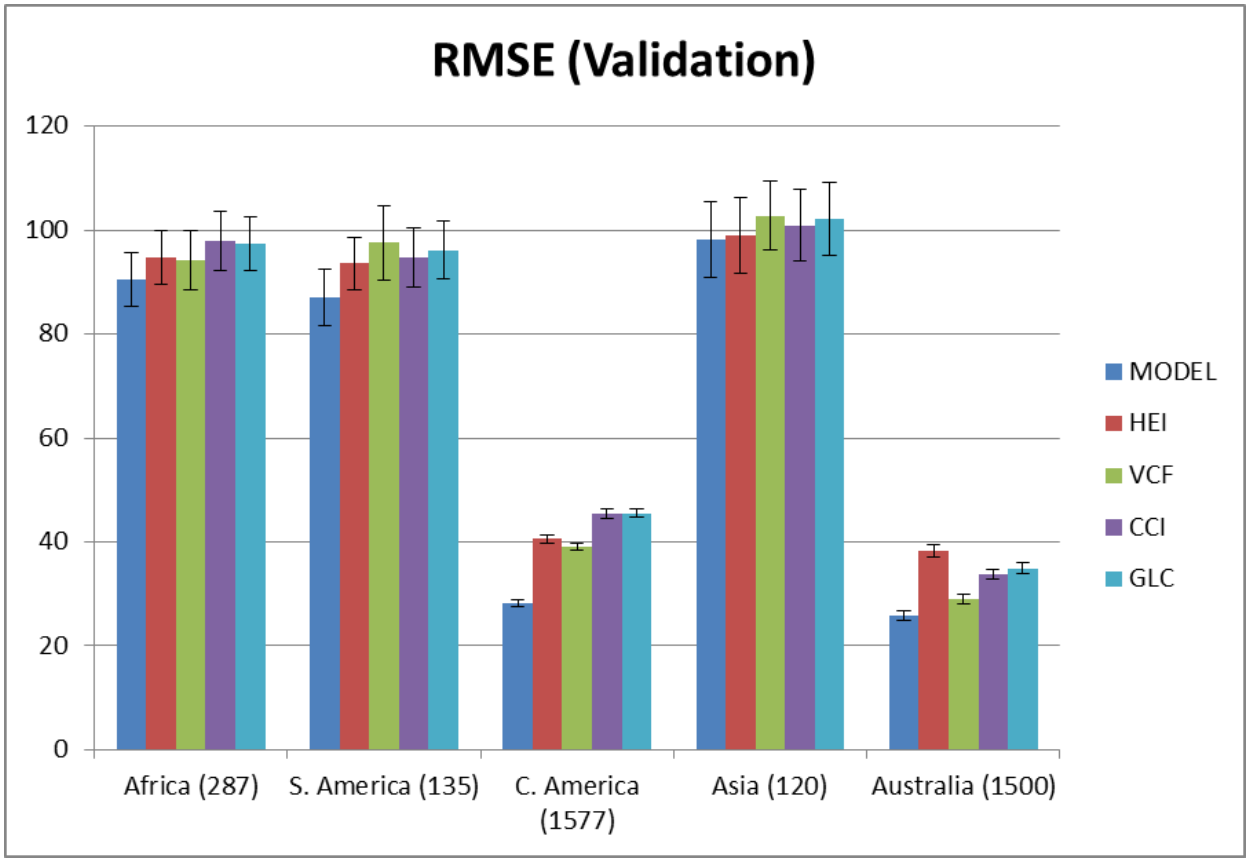

Figure S5: Performance of all stratification approaches, computed as RMSE of the respective fused maps assessed using independent reference data. The "Model" stratification refers to the approach used in this study ("Error strata"). The alternative stratification approaches consist of individual datasets used to predict the errors of the input maps, i.e., forest height ("HEI"), tree cover ("VCF"), land cover according to the GLC2000 map ("GLC") and land cover according to the ESA CCI map ("CCI").

Reference dataset

Visual selection of the reference field data

After the preliminary selection of field plots based on metadata information (tree parameters measured in the field, allometric model applied, year of measurement, plot geolocation and extent), the ground data were further screened to discard the plots not representative of the biomass density within the 1 km cells of the input maps. Considering that the two input maps are not aligned and therefore their pixels do not correspond to the same geographic area, the plots needed to be representative of the area of both pixels identified before their resampling. For this reason, the plot representativeness was assessed on the area obtained by merging the pixel extent of the Saatchi map with the corresponding pixel extent of the Baccini map after its aggregation to 1 km but before its resampling. The representativeness was assessed by means of visual interpretation of high resolution images provided on the Google Earth platform, discarding the plots located in pixels with

heterogeneous tree cover and tree crowns. Pixels were considered heterogeneous if more than 10% of the area presented forest structure different than that of the majority of the area (i.e., pixels needed to be homogeneous for at least 90% of their area). Moreover, if the sum of the area of all plots located within a pixel was smaller than 0.1 ha, these plots were removed because the area measured on the ground was considered insufficient to represent 1km pixels even in homogeneous contexts. Even though biomass may still vary substantially within an area having similar forest structure, using the texture and context information assessed through visual interpretation allowed for higher confidence than assessing pixel homogeneity using fixed thresholds of tree cover and texture variability automatically derived from coarser resolution images (i.e., MODIS or Landsat). Examples of plots selected or discarded through the visual analysis of Google Earth images are provided in Fig. S6.

Figure S6: visual selection of the field plots. Plots are discarded if not representative of the biomass density in the 1 km^2 area of the input maps. The yellow and red polygons represent the area of the corresponding pixels of the Saatchi and Baccini maps and the blue circles represent the extent of the field plots, superimposed on the Google Earth images. The right plots were selected (tree cover and texture are homogeneous) and the left plot was discarded (heterogeneous pixels). *FIGURE TO BE ENHANCED: plot area is not visible*

The pan-tropical reference dataset

The reference data selected after the screening, upscaling and consolidating procedure, for each individual dataset are reported in Table S2. The field plots underpinning the reference biomass maps are not included among the "Available plots" to avoid double-counting, since the respective reference data are already considered as "Selected pixels". Table S3 indicates the main type of training data used by the high resolution biomass maps and the criteria used to select the 1-km

reference pixels for this study. A complete description of the metadata and the literature reference of the ground reference data and reference biomass maps are provided in Table S7 – S10.

Table S2: Number of reference data (plots and 1-km pixels) selected after the screening, upscaling and consolidating procedure, for each individual dataset.

ID	Continent	Type	Country/Region	Available	Selected		Consolidated
				Plots	Plots	Pixels	Pixels
AFR1	Africa	Plots	DRC	1,157	1,067	227	227
AFR2	Africa	Plots	Sierra Leone	609	576	162	162
AFR3	Africa	Plots	Tropical Africa	260	175[(a)]	161	161
AFR4	Africa	Plots	Ethiopia	119	60	42	42
AFR5	Africa	Plots	Ghana	74	65	12	12
AFR6	Africa	Plots	Tanzania	42	23	9	9
AFR7	Africa	Plots	DRC	20	10	9	9
AFR8	Africa	Map	Uganda			223	223
AFR9	Africa	Map	Madagascar			60	60
AFR10	Africa	Map	Mozambique			38	38
AFR11	Africa	Map	Cameroon			10	10
TOTAL AFRICA				**2,281**	**1,976**	**953**	**953**
SAM1	S. America	Plots	Amazon basin	413	287[(b)]	221	221
SAM2	S. America	Plots	Brazil	124	101	48	48
SAM3	S. America	Plots	Guyana	111	86	30	30
SAM4	S. America	Map	Peru			100	100
SAM5	S. America	Map	Colombia			50	50
TOTAL S. AMERICA				**648**	**474**	**449**	**449**
CAM1	C. America	Map	Mexico			4,263	6,072
CAM2	C. America	Map	Panama			997	3,095
TOTAL C. AMERICA				**0**	**0**	**5,260**	**9,167**
ASI1	Asia	Plots	Vietnam	3,197	1,547	101	101
ASI2	Asia	Plots	Laos	122	68	65	65
ASI3	Asia	Plots	Sabah	104	74	53	53
ASI4	Asia	Plots	Indonesia	82	39	36	36
ASI5	Asia	Plots	SE Asia	132	77	77	77
ASI6	Asia	Plots	Indonesia	25	17	11	11

ASI7	Asia	Plots	SE Asia	25	4	4	4
ASI8	Asia	Plots	Indonesia	11	7	6	6
ASI9	Asia	Map	Asia			0	47[(c)]
TOTAL ASIA				**3,698**	**1,833**	**353**	**400**
AUS1	Australia	Map	Australia			5,000	5,000
TOTAL AUSTRALIA				**0**	**0**	**5,000**	**5,000**
TOTAL TROPICS				**6,627**	**4,283**	**12,015**	**15,969**

[(a)] 22 plots (DOU, OVG, EKO, LOP-01, CVL, GBO) were removed because they were used by Saatchi et al. (2011) to calibrate the LiDAR/biomass relationships, and therefore highly correlated with the map values.

[(b)] 264 plots measured for the last time after the year 2000 were selected. In addition, 23 plots measured from 1990 in undisturbed forests were included because the visual analysis of high-resolution images did not indicate any sign of disturbance.

[(c)] Additional training data representing areas with no biomass (e.g., bare soil) were included only for Asia, where 47 pixels were selected using visual analysis of Google Earth images.

Table S3: Type of calibration data used by the high resolution biomass maps (identified by the "ID") and criteria used to select the 1-km reference pixels for this study ("Selected pixels").

ID	Calibration data	Selected pixels
AFR8	Field plots	Pixels with plots representative of >40% of pixel area
AFR9	Airborne LiDAR	Random pixels in an amount proportional to other datasets
AFR10	Field plots	All pixels with plots
AFR11	Field plots	All pixels with plots
SAM4	Airborne LiDAR	Random pixels in an amount proportional to other datasets
SAM5	Airborne LiDAR	Random pixels in an amount proportional to other datasets
CAM2	Field plots	Pixels with available plots
CAM3	Airborne LiDAR	Random pixels in an amount proportional to the map area
AUS1	Field plots	Random pixels in an amount proportional to other continents

The reference dataset described above was used to assess the errors of the input maps (RMSE) and the linear correlation (r) of the errors for each continent (Table S4).

Table S4: Linear correlation of the errors (r) and RMSE of the input maps computed using the complete reference dataset, per continent.

	Africa	S. America	C. America	Asia	Australia

	Saatchi	Baccini	Saatchi	Baccini	Saatchi	Baccini	Saatchi	Baccini	Saatchi
r	0.77	0.72	0.61	0.65	0.60	0.75	0.64	0.72	0.69
RMSE	105	116	104	96	97	101	124	103	45

The fusion model

The biases and weights computed by the fusion model per stratum and continent are reported in Table S5, along with the number of reference data and relative area of each stratum (in percentage).

Table S5: Bias values and weights applied to the input maps, number of reference data and percentage relative area per stratum and continent

	Bias		Weight		Ref. data (N)	Area
Strata	**Saatchi**	**Baccini**	**Saatchi**	**Baccini**		
AFRICA						
1	-11	-55	0.29	0.71	111	13%
2	-26	-17	0.57	0.43	123	21%
3	113	203	0.54	0.46	163	1%
4	200	146	0.00	1.00	77	2%
5	77	-51	0.93	0.07	66	3%
6	-91	-49	0.07	0.93	146	7%
7	-56	-87	0.45	0.55	89	8%
8	-7	16	0.60	0.40	178	45%
ASIA						
1	-42	-22	0.75	0.25	83	69%
2	82	52	0.00	1.00	19	2%
3	43	116	0.45	0.55	26	2%
4	174	190	0.00	1.00	38	2%
5	-186	-74	0.84	0.16	74	2%
6	-125	-117	0.43	0.57	61	2%
7	11	-31	1.00	0.00	55	14%
8	-77	20	1.00	0.00	44	6%
CENTRAL AMERICA						
1	-16	-67	0.43	0.57	1574	20%
2	-12	-112	0.34	0.66	1155	7%
3	-119	-80	0.62	0.38	1511	6%
4	-76	-163	0.53	0.47	748	2%
5	-204	-101	0.45	0.55	617	3%
6	-63	-74	0.65	0.35	2402	9%
7	-14	-27	0.38	0.62	637	51%
8	-178	-178	0.33	0.67	506	1%

SOUTH AMERICA						
1	-37	-112	0.38	0.62	72	6%
2	27	5	0.84	0.16	43	10%
3	-18	-44	0.96	0.04	37	56%
4	38	-64	0.39	0.61	51	7%
5	161	139	0.17	0.83	79	3%
6	-102	-79	0.75	0.25	59	4%
7	-23	3	0.33	0.67	48	10%
8	124	40	0.97	0.03	60	5%
AUSTRALIA						
1	-21	NA	1.00	0.00	847	16%
2	-37	NA	1.00	0.00	449	6%
3	79	NA	1.00	0.00	411	2%
4	2	NA	1.00	0.00	859	29%
5	141	NA	1.00	0.00	220	2%
6	41	NA	1.00	0.00	564	4%
7	-11	NA	1.00	0.00	1145	35%
8	16	NA	1.00	0.00	505	6%

Biomass map

Biomass stocks of the fused and input maps

The total biomass stocks (Pg) of all land cover types per continent and biomass map are reported in Table S6. For comparability among the three maps (Saatchi, Baccini and fused map), the stocks are computed for the extent of the Baccini map while the values in brackets represent the stocks relative to the larger extent of the Saatchi map. The values reported for the Saatchi map are higher than those published by Saatchi et al. (2011) because the latter refer only to areas with tree canopy cover >10%.

Table S6: Total biomass stocks (Pg) of all land cover types per continent and biomass map. The values refer to the extent of the Baccini map while the values in brackets represent the stocks relative to the larger extent of the Saatchi map.

	Africa	S. America	C. America	Asia	Australia	Total
Baccini	129	216	18	93	-	457
Saatchi	113 (117)	178 (196)	15 (20)	107 (192)	(21)	413 (545)
Fused	96 (97)	179 (191)	7 (9)	78 (134)	(19)	360 (451)

Comparison of forest biomass in intact and non-intact landscapes

The biomass values per continent for intact and non-intact forests were computed as the area-weighted mean of the contributing ecozones (see related section in "Data and Methods"). In Africa the fused map presented higher mean biomass values than the Saatchi and Baccini maps in intact forests (+86 and +65 Mg ha^{-1}, respectively) and lower values in non-intact forests (-15 and -36 Mg ha^{-1}, respectively), in Asia and in Central America the fused map was consistently lower than the input maps in both intact (between -74 and -125 Mg ha^{-1}) and non-intact forests (between -51 and -65 Mg ha^{-1}), in South America the fused map was similar to the Saatchi map in both intact and non-intact forests (+20 and +3 Mg ha^{-1}, respectively) and lower than the Baccini map (-18 and -28 Mg ha^{-1}, respectively), and in Australia the fused map was higher than the Saatchi map in both intact and non-intact forests (+72 and +30 Mg ha^{-1}, respectively). As expected, intact forests had consistently higher mean biomass than non-intact forest in all continents and major ecozones. When considering the average difference between intact and non-intact forests, this was larger in the fused map than in the Saatchi and Baccini maps in Africa (236, 143 and 154 Mg ha^{-1} respectively), similar or slightly larger in South America (78, 63 and 79 Mg ha^{-1} respectively), and smaller in Central America (58, 74 and 86 Mg ha^{-1} respectively) and Asia (39, 59 and 55 Mg ha^{-1} respectively).

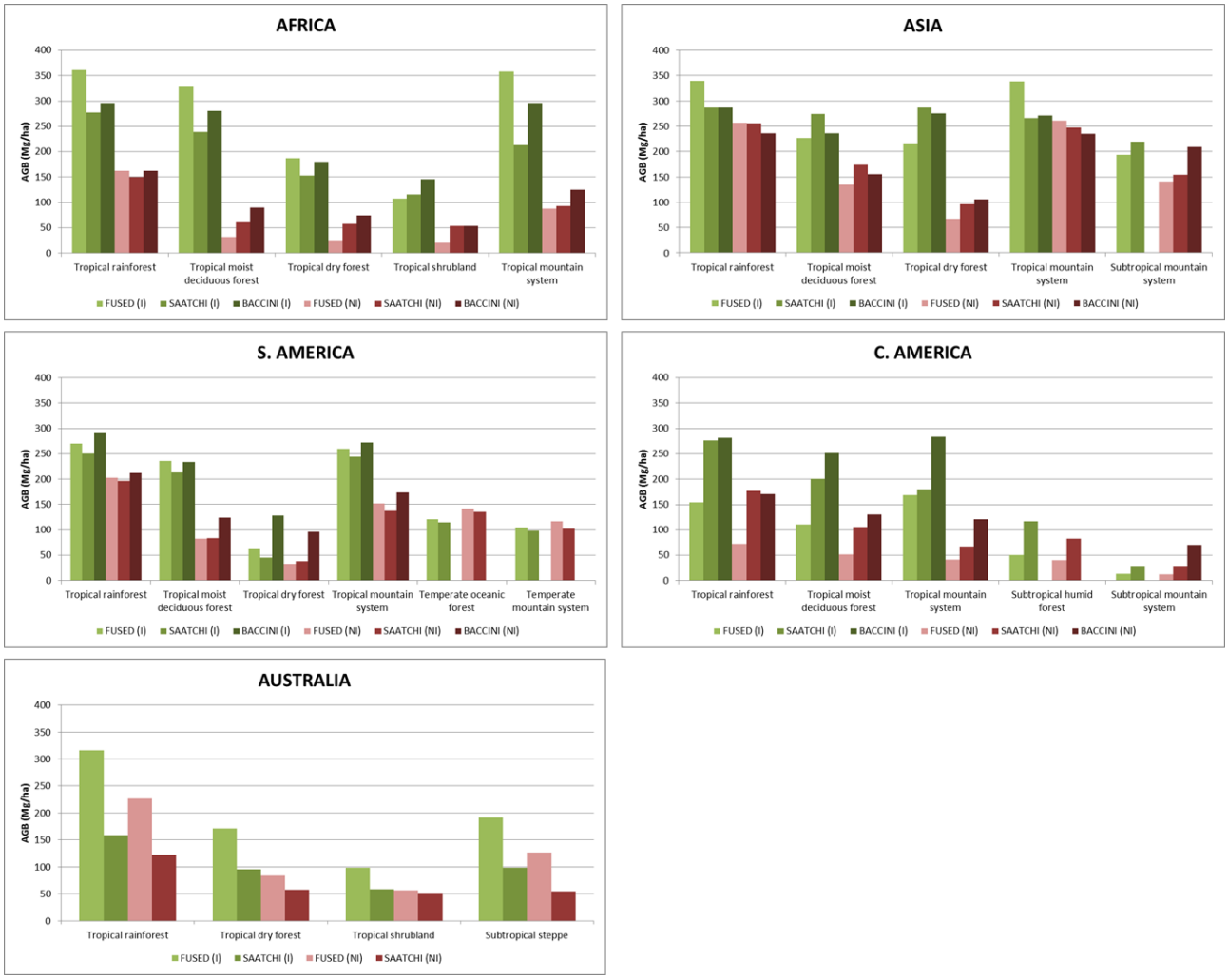

Figure S7: Mean biomass density of the fused and input maps in intact (I) and non-intact (NI) forests stratified by continent and ecozone. Only ecozones with intact forest larger than 1,000 km^2 are reported

Table S7: Metadata of the ground reference datasets (part 1)

ID	Continent	Country / Region	Location	Extent	Vegetation type(s)	Year(s)	N. plots	Area - Range (ha)	Area - Mean (ha)	Min. DBH (cm)	Referen
AFR1	Africa	DRC	Lukenie	Local	Forest (concession)	NA	1157	0.5	0.5	10	Hirsch et al., 2013
AFR2	Africa	Sierra Leone	Gola Forest	Local	Forest	2005-2007	609	0.125	0.125	10	Lindsell and Klop, 201
AFR3	Africa	Tropical Africa	Tropical Africa	Regional	Forest (Intact)	1970s - 2013	260	0.2 - 10	1.2	10	Lewis et al., 2013
AFR4	Africa	Ethiopia	Kafa	Local	Forest - Woodland	2011-2013	119	0.126	0.126	5	De Vries et al., 2012
AFR5	Africa	Ghana	Ankasa	Local	Forest	2012	34	0.05	0.05	10	Laurin et al., 2013
AFR5	Africa	Ghana	Bia Boin, Dadieso	Local	Forest	2012-2013	40	0.16	0.16	5	Pirotti et al., 2014
AFR6	Africa	Tanzania	Eastern Arc Mountain	Local	Forest	2007-10	42	0.08 - 1	0.66	10	Lopez-Gonzalez et al.
AFR7	Africa	DRC	Yangambi	Local	Forest (Intact)	NA	20	1	1	10	Kearsley et al., 2013
SAM1	S. America	Amazon	Amazon	Regional	Forest	1956 - 2013	413	0.25 - 9	1	10	Mitchard et al., 2013; Gonzalez et al., 2014
SAM2	S. America	Brazil	Brazil	National	Forest	2009 - 2013	124	0.16 - 1	0.42	5 - 10	Embrapa, 2014
SAM3	S. America	Guyana	Guyana	Local	Forest	2010 - 2011	111			5	NA
CAM1	*C. America*	*Mexico*	*Mexico*	*National*	*Forest*	*2004-2008*	*4136*			*7.5*	*de Jong, 2013*
ASI1a	Asia	Vietnam	Quang Nam	Province	Forest	2007-2009	3035	0.05	0.05	6	Avitabile et al., 2014
ASI1b	Asia	Vietnam	Quang Nam	Province	Forest	2011-2012	162	0.01 - 0.126	0.08	5	Avitabile et al., 2014
ASI2	Asia	Laos	Xe Pian	Local	Forest	2011-2012	122	0.1 - 0.126	0.11	5	WWF and OBf, 2013
ASI3	Asia	Indonesia	Sabah	Local	Forest (concession)	2005 - 2008	104	0.5 - 1.5	1	10	Morel et al., 2011
ASI4	Asia	Indonesia	Riau province	Local	Forest	2009-2010	82	0.015	0.015	5	Wijaya et al., 2015
ASI5	Asia	Asia	India, China, Indonesia	Local	Forest (Intact)	circa-2010	132	0.25 - 20	1.5	10	Slik et al., 2013, 2014
ASI6	Asia	Malaysia, Indonesia	Sarawak, C. Kalimantan	Regional	Forest (Intact)	2013 - 2014	25	0.25 - 1	0.57	10	Phillips et al., in prep
ASI7	Asia	Indo-Pacific	Indo-Pacific	Regional	Mangrove	2008 - 2009	25	0.015	0.015	5	Donato et al., 2011
ASI8	Asia	Indonesia	Kalimantan	Local	Mangrove	2008-2009	11	0.015	0.015	5	Murdiyarso et al., 20

[(a)] The metadata for this dataset are provided in Amira (2008) and Kauffman and Donato (2012)

Table S8: Metadata of the ground reference datasets (part 2)

ID	Parameter measured	Tree Height	Allometric equation	Parameters of allom. eq.	Plot type	Permanent plot
AFR1	Dbh, Sp, Hei	not used	Chave (2005) Moist	Dbh, wd, hei	For. Inv.	No
AFR2	Dbh, Sp, Hei	local eq.	Chave (2005) Moist	Dbh,wd, hei	For. Inv.	No
AFR3	Dbh, Sp	Feldpausch (2012)	Chave (2005) Moist	Dbh,wd, hei	Res. plots	Yes
AFR4	Dbh, Sp	not used	Chave (2005) Wet	dbh, wd	Res. plots	No
AFR5	Dbh, Sp, Hei	measured for all trees	Chave (2005) Moist	Dbh,wd, hei	Res. plots	No
AFR5	Dbh, Sp, Hei	measured for all trees	Chave (2005) Moist	Dbh,wd, hei	Res. plots	No
AFR6	Dbh, Sp	Feldpausch (2012)	Chave (2005) Moist	Dbh,wd, hei	Res. plots	Yes
AFR7	Dbh, Sp, Hei	stand-specific eq.	Chave (2005) Moist	Dbh,wd, hei	Res. plots	Yes
SAM1	Dbh, Sp	Feldpausch (2012)	Chave (2005) Moist	Dbh,wd, hei	Res. plots	Yes
SAM2	Dbh, Sp, Hei	measured for all trees	Chave (2005) Moist	Dbh,wd, hei	For. Inv.	No
SAM3	Dbh, Sp	not used	Chave (2005) Moist	*dbh, wd*	For. Inv.	No
CAM1	*Dbh, Sp, Hei*	*measured for all trees*	*Urquiza-Haas et al. (2007)*	*Dbh,wd, hei*	*For. Inv.*	*Yes*
ASI1a	Dbh, Sp, Hei	local eq.	Chave (2005) Moist	Dbh,wd, hei	For. Inv.	No
ASI1b	Dbh, Sp	not used	Chave (2005) Moist	dbh, wd	Res. plots	No
ASI2	Dbh, Sp	not used	Chave (2005) Dry/Moist	dbh, wd	Res. plots	No
ASI3	Dbh, Sp, Hei	stand-specific eq.	Chave (2005) Moist	Dbh,wd, hei	Res. plots	No
ASI4	Dbh, Sp	not used	Komiyama et al. (2008), Chave (2005) Moist	dbh, wd	Res. plots	No
ASI5	Dbh, sp	Feldpausch (2012)	Chave (2005) Dry/Moist/Wet	Dbh,wd, hei	Res. plots	No
ASI6	Dbh, sp	Feldpausch (2012)	Chave (2005) Moist	Dbh,wd, hei	Res. plots	Yes
ASI7	Dbh, sp	not used	Komiyama et al. (2008)	dbh, wd	Res. plots	No
ASI8	Dbh, Sp	not used	Komiyama et al. (2008)	dbh, wd	Res. plots	No

Table S9: Metadata of the reference biomass maps (part 1)

ID	Continent	Country/Region	Location	Extent	Vegetation types [a]	Year (map)	Resolution (m)	Accuracy dataset	RMSE (Mg/ha)	R2	RS data	Reference
AFR8	Africa	Uganda	Uganda	National	For – Wood – Sav.	1999-2003	30	Validation	13	0.81	Landsat, LC	Avitabile et al., 2012
AFR9	Africa	Madagascar	North Madagascar	Local	Forest	2010	100	Calibration	42	0.88	Landsat, LiDAR	Asner et al., 2012
AFR10	Africa	Mozambique	Gorongosa	Local	Wood – Sav	2007	50	Validation	20	0.49	ALOS	Ryan et al., 2012
AFR11	Africa	Cameroon	Mbam Djerem	Local	For - Sav	2007	100	Calibration	29	NA	ALOS	Mitchard et al., 2011
SAM4	S. America	Peru	Peru	National	For – Wood – Grass	NA	100	Calibration	55	0.82	Landsat, LiDAR	Asner et al., 2014
SAM5	S. America	Colombia	Colombian amazon	Regional	Forest	2010	100	Validation	58	NA	Landsat, LiDAR	Asner et al., 2012
CAM2	C. America	Mexico	Mexico	National	Forest	2007	30	Validation	28	0.52	Landsat, ALOS	Cartus et al., 2014
CAM3	C. America	Panama	Panama	National	For – Wood – Grass	2008 - 2012	100		45	0.62	Landsat, LiDAR	Asner et al., 2013
AUS1	Australia	Australia	West Australia	Local	Wood – Sav		50	NA	NA	NA	ALOS	Lucas et al., 2010

[a]) Forest (For), woodland (Wood), Savannah (Sav), Grassland (Grass)

Table S10: Metadata of the reference biomass maps (part 2)

ID	N. plots	Years (Plots)	Plot size - Range (ha)	Plot size - Mean (ha)	Min. DBH (cm)	Parameter measured	Tree Height	Allometric equation	Parameters of allometric eq.	Plot type
AFR8	2527	1995-2005	0.25	0.25	3	Dbh, Sp, Crown	measured	Drichi (2003)	Dbh, wd, crown	For. Inv.
AFR9	19	NA	0.28	0.28	0	Dbh, Sp, Hei	local eq.	Chave (2005) Wet	Dbh, wd, hei	Res. plots
AFR10	96	2006-2009	0.1 - 2.2	0.63	5	Dbh	not used	Ryan et al. (2011)	dbh	Res. plots
AFR11	25	2007	0.2 - 1	0.6	10	Dbh, Sp, Hei	local eq.	Chave (2005) Dry/Moist/Wet	Dbh, wd, hei	Res. plots
SAM4	272	NA	0.3 - 1	0.33	NA	Dbh, Sp, Hei	local eq.	Chave et al., 2014	Dbh, wd, hei	For. Inv.
SAM5	11	NA	0.28	0.28	10	Dbh, Sp	local eq.	Chave (2005) Moist	Dbh, wd, hei	Res. plots
CAM2	16906	2004 - 2007	1	1	7.5	Dbh, Sp, Hei	measured	National species-specific eq.	Dbh, wd, hei	For. Inv.
CAM3	228	NA	0.1 - 0.36	NA	10	Dbh, Sp, Hei	local eq.	Chave (2005) Dry/Moist/Wet	Dbh, wd, hei	Res. plots
AUS1	2781									

Additional References

Amira S (2008). An estimation of Rhizophora apiculata Bl. biomass in mangrove forest in Batu Ampar Kubu Raya Regency, West Kalimantan. Undergraduate Thesis, Bogor Agricultural University, Indonesia

Avitabile V, 2014. Carbon stocks of vegetation in the Vu Gia Thu Bon river basin, central Vietnam. Technical Report. Land Use and Climate Change Interactions in Central Vietnam (LUCCi) project. http://leutra.geogr.uni-jena.de/vgtbRBIS/metadata/start.php

DeVries B, Avitabile V, Kooistra L, Herold M, 2012. Monitoring the impact of REDD+ implementation in the Unesco Kafa biosphere reserve, Ethiopia. Proceedings of the "Sensing a Changing World" Workshop (2012).http://www.wageningenur.nl/upload_mm/9/d/c/f80b6db7-9c3c-4957-8717-6fdc6e46e60f_deVries.pdf

Donato DC, Kauffman JB, Murdiyarso D, Kurnianto S, Stidham M, Kanninen M (2011) Mangroves among the most carbon-rich forests in the tropics. *Nature Geoscience*, **4**, 293–297.

EMBRAPA, 2014. Sustainable Landscape Brazil. http://geoinfo.cnpm.embrapa.br/geonetwork/srv/eng/main.home

ESA, 2014. Global land cover map for the epoch 2005. http://www.esa-landcover-cci.org/

DiMiceli, C.M., Carroll, M.L., Sohlberg, R.A., Huang, C., Hansen, M.C. and Townshend J.R.G. (2011). Annual Global Automated MODIS Vegetation Continuous Fields (MOD44B) at 250 m Spatial Resolution for Data Years Beginning Day 65, 2000 - 2010, Collection 5 Percent Tree Cover, University of Maryland, College Park, MD, USA

Hirsh, F.; Jourget, J. G.; Feintrenie, L.; Bayol, N.; Atyi, R. E., 2013. REDD+ pilot project in Lukenie. Center for International Forestry Research (CIFOR), Jakarta, Indonesia, CIFOR Working Paper, 2013, 111, pp vi + 48 .

Jung M, Henkel K, Herold M, Churkina G (2006) Exploiting synergies of global land cover products for carbon cycle modeling. *Remote Sensing of Environment*, **101**, 534–553.

Kauffman JB and Donato DC (2012). Protocols for the measurement, monitoring and reporting of structure, biomass and carbon stocks in mangrove forests. Working Paper 86. CIFOR, Bogor, Indonesia.

Liaw, A., Wiener, M. (2002). Classification and regression by random forest. R News, 2 (3), 18–22.

Lindsell J a., Klop E (2013) Spatial and temporal variation of carbon stocks in a lowland tropical forest in West Africa. *Forest Ecology and Management*, **289**, 10–17.

Lopez-Gonzalez, G., Lewis, S.L., Burkitt, M., Baker T.R. and Phillips, O.L. 2009. ForestPlots.net Database. www.forestplots.net. Date of extraction [09,09,13]

Lopez-Gonzalez G, Lewis SL, Burkitt M and Phillips OL (2011). ForestPlots.net: a web application and research tool to manage and analyse tropical forest plot data. Journal of Vegetation Science 22: 610–613. doi: 10.1111/j.1654-1103.2011.01312.x

Lopez-Gonzalez G, Mitchard ETA, Feldpausch TR et al. (2014) Amazon forest biomass measured in inventory plots. Plot Data from "Markedly divergent estimates of Amazon forest carbon density from ground plots and satellites." doi: 10.5521/FORESTPLOTS.NET/2014_1

Lucas R, Armston J, Fairfax R et al. (2010). An evaluation of the ALOS PALSAR L-band backscatter – above ground biomass relationship over Queensland, Australia. *IEEE Journal of Selected Topics in Earth Observations and Remote Sensing*, 3(4): 576-593.

Mayaux P, Bartholome E, Fritz S, Belward A (2004) A New Land Cover Map of Africa for the Year 2000. *Journal of Biogeography*, **31**, 861–877.

Mitchard ET, Saatchi SS, Lewis SL et al. (2011) Measuring biomass changes due to woody encroachment and deforestation/degradation in a forest-savanna boundary region of central Africa using multi-temporal L-band radar backscatter. *Remote Sensing of Environment*, **115**, 2861–2873.

Morel AC, Saatchi SS, Malhi Y et al. (2011) Estimating aboveground biomass in forest and oil palm plantation in Sabah, Malaysian Borneo using ALOS PALSAR data. *Forest Ecology and Management*, **262**, 1786–1798.

Murdiyarso D, Donato D, Kauffman JB, Kurnianto S, Stidham M, Kanninen M (2010). Carbon storage in mangrove and peatland ecosystems: a preliminary account from plots in Indonesia. *CIFOR Working Paper no. 48*. 35pp. Bogor – Indonesia.

Phillips O.L., Lewis S.L., Qie L., Banin L., et al. (in prep.) Tropical Forests in the Changing Earth System Borneo forest dataset'.

Pirotti F, Laurin G, Vettore A, Masiero A, Valentini R (2014) Small Footprint Full-Waveform Metrics Contribution to the Prediction of Biomass in Tropical Forests. *Remote Sensing*, 9576–9599.

Ryan CM, Hill T, Woollen E et al. (2012) Quantifying small-scale deforestation and forest degradation in African woodlands using radar imagery. *Global Change Biology*, **18**, 243–257.

Simard M, Pinto N, Fisher JB, Baccini A (2011) Mapping forest canopy height globally with spaceborne lidar. Journal of Geophysical Research: Biogeosciences, 116, 1–12.

Vaglio Laurin G, Chen Q, Lindsell J, Coomes D, Cazzolla-Gatti R, Grieco E, Valentini R (2013) Above ground biomass estimation from lidar and hyperspectral airbone data in West African moist forests. *EGU General Assembly Conference Abstracts*, **15**, 6227.

Wijaya A, Liesenberg V, Susanti A, Karyanto O, Verchot LV (2015). Estimation of Biomass Carbon Stocks over Peat Swamp Forests using Multi-Temporal and Multi-Polarizations SAR Data. *Proceeding of the 36th International Symposium on Remote Sensing of Environment*, 11-15 May 2015, Berlin, Germany.

WWF and ÖBf. 2013. Xe Pian REDD+ project document. Gland, Switzerland. http://www.leafasia.org/sites/default/files/public/resources/WWF-REDD-pres-July-2013-v3.pdf